BABEȘ-BOLYAI UNIVERSITY, CLUJ-NAPOCA **Year 2022**
UNIVERSITY OF BUCHAREST, BUCHAREST

Exploring supramolecular interactions for rotaxanes synthesis and modulation of optical and electronic properties of oligothiophene and 1,3,4-oxadiazole derivatives

PhD THESIS in Organic Chemistry
Doctoral School of Chemistry
Faculty of Chemistry and Chemical Engineering, Cluj-Napoca
Public defense 4th November 2022
Cluj-Napoca
by Cătălin-Constantin Anghel

Jury

President:	***Acad. Cristian Silvestru***	***Babeș-Bolyai University, Cluj-Napoca, Romania***
Scientific advisors:	***Prof. Dr. Ion Grosu***	***Babeș-Bolyai University, Cluj-Napoca, Romania***
	Acad. Marius Andruh	***Romanian Academy, Bucharest, Romania***
Reviewers:	***Dr. Mihail Bărboiu***	***European Membrane Institute, Montpellier, France***
	Dr. Mihaela Florea	***National Institute of Materials Physics, Bucharest Măgurele, Romania***
	Conf. Dr. Augustin Mădălan	***University of Bucharest, Romania***
	Conf. Dr. Habil. Niculina Hădade	***Babeș-Bolyai University, Cluj-Napoca, Romania***

Table of Contents

Keywords: organic solar cells, acceptors, single-material organic solar cells, 1,3,4-oxadiazole, ESIPT, ESPT, rotaxanes, mechanically interlocked molecules.

General introduction

The thesis is structured in three distinct parts and it presents contributions brought in the field of organic compounds with electronic properties for Organic Light Emitting Diodes (OLEDs) and Organic Solar Cells (OSCs), as well as the field of mechanically interlocked molecules.

The first chapter presents a detailed study of the photoelectronic and photovoltaic properties of new organic semiconductors for OSCs. In the first subchapter, we have attempted the synthesis of a rigidified terthiophene **1.2a** equivalent of the indacenedithiophene **1.1**, a widely employed non-fullerene acceptor in the construction of OSCs. Both the experimental and the theoretical work proved the unexpected formation of a naphtho[2,3-*b*]thiophene **1.2b**. In the second subchapter we have continued the development of thiophene based acceptors: terthiophene diesters **1.3** and hexathiophene tetraesters **1.4**. The last subchapter presents results regarding the use of triarylamine donors as materials for Single Component Organic Solar Cells (SCOSCs).

The second chapter is concentrated on the synthesis and the characterization of new hydroxy functionalized 1,3,4-oxadiazoles. The first subchapter presents the study of mono oxadiazoles **2.1** and **2.2** that exhibit excited state intermolecular proton transfer (ESPT) and excited state intramolecular proton transfer (ESIPT) in solution and solid state. It also presents their application as hydrogen bond donor in the building of three new organic cocrystals. The second subchapter discusses the optical properties of hydroxy bis-oxadiazoles **2.3** and **2.4**, in solution and solid state.

In the third chapter a new method to form [2]rotaxanes is described, metal active CuAAC clipping. The axle of the rotaxane contains two types of functional groups (stations): triazole and pyridine. A commercial copper(I) reagent ($Cu(CH_3CN)_4PF_6$) and a carbene based reagent [CuCl(SIMes)] were employed as copper sources. The clipping reaction was either intramolecular or a [1+1] macrocyclization, the first one providing better results.

Chapter 1. Organic materials for solar cells

1.1 Introduction

Humanity is being confronted with a wide range of crises from which the energy consumption easily stands out.[1] In this context, the development of the photovoltaics, and implicitly of organic photovoltaics (OPV) is required to make use of the solar energy, which is a renewable source of energy.[2] The most efficient Organic Solar Cells (OSCs) generally contain two components: a donor and an acceptor. The go-to acceptors were based on the fullerene moiety, but the efforts in this domain led to more efficient non-fullerene acceptors (NFAs).[3]

1.2 Results and discussion

Given the importance of the organic solar cells, we have decided to direct our efforts towards developing new compounds to be used as small molecule NFAs for OSCs, as well as modifying already known structures in order to improve their properties. The first part is discussing the attempted synthesis of a rigidified terthiophene **1.2a** as donor moiety for NFAs, which instead led to the formation of the napththo[2,3-b]thiophene **1.2b**.[4] In the second part we have targeted other small molecules as NFAs for OSCs based on the structure of terthiophene diester **1.3** and of the hexathiophenes **1.4a**,**b**.

The last subject presents my contributions to a collaborative project with fellow PhD students concerning the use of small conjugated molecules, based on triphenylamine (TPA) compounds, as single material for SMOSCs.

1.2.1 Synthesis of terthiophene diesters

In order to obtain the NFAs acceptors we had to firstly synthesize a series of terthiophene diesters **1.8** (**Schemes 1.1 and 1.2**), which were next used as building blocks for different NFAs. The first target **1.8a** (**Scheme 1.1**) were needed for the attempted synthesis of **1.2a**, as well as for the synthesis of **1.3a**. The second target **1.8b** was synthesized in order to improve the solubility of the final compound. The synthetic pathway consists of three steps: esterification of 3,4-thiophenedicarboxylic acid with the corresponding alcohol, the bromination of the ester with bromine/AcOH, followed by a Stille reaction with 2-(tri-n-butylstannyl)thiophene, catalyzed by $Pd(PPh_3)_4$.

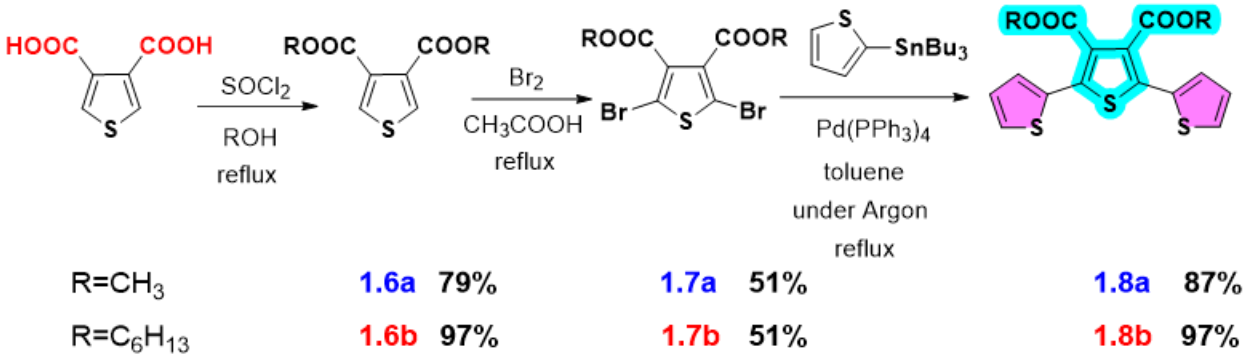

Scheme 1.1 The synthesis of the vicinal terthiophene diesters **1.8**

The last thiophene-based intermediate **1.8c** (**Scheme 1. 3**) was necessary in order to test alternative paths towards the synthesis of compound **1.2a.** The synthesis of **1.8c** required 2-bromo-3-thiophenecarboxylic acid (**1.10**) which was esterified by following the same method presented for **1.6a**. The second step was a Stille reaction between ester **1.11** and 2,5-di(tributylstannyl)thiophene and it had a good yield of 62% (**Scheme 1.2**).

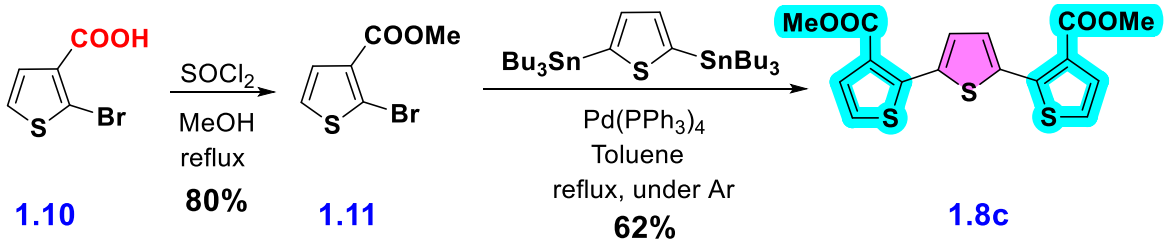

Scheme 1. 2 Synthesis of the distal terthiophene diester **1.8c**

1.2.2 Rigidified terthiophene based NFA: unexpected synthesis of a naphtho[2,3-b]thiophene

The synthetic strategy of compound **1.2a** (**Figure 1.1**) started from the ester **1.8a**, or from ester **1.8c** as an alternative strategy.

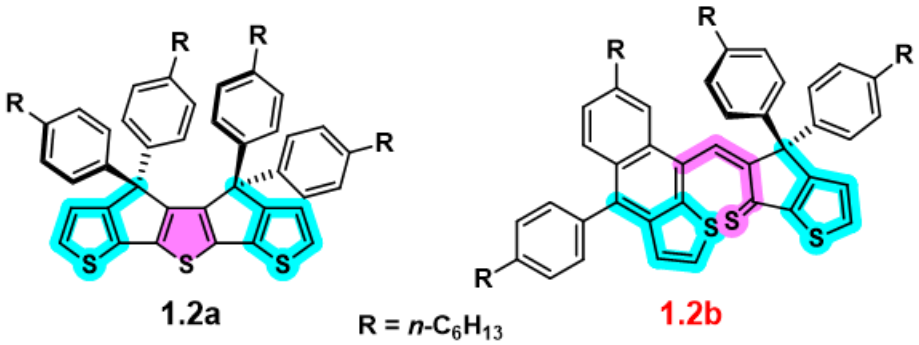

Figure 1.1 The structure of the target compound **1.2a** and the unexpected naphtho[2,3-b]thiophene derivative **1.2b** obtained

The steric hindrance presented by four alkylaryl fragments in close proximity forced the breaking of the central thiophene to form **1.2b** instead of the target compound **1.2a** (**Figure 1.1**).

1.2.2.1 Synthesis of the naphtho[2,3-b]thiophene 1.2b

The synthesis of compound **1.12a** from diester **1.8a** was attempted by a Grignard reaction. This led to the formation of diketone **1.13a** in a very high yield 90%. Ketoalcohol **1.13b** is obtained in a considerable yield 22% together with the ketone in a 70% yield when the mixture is refluxed overnight (**Scheme 1.4**).

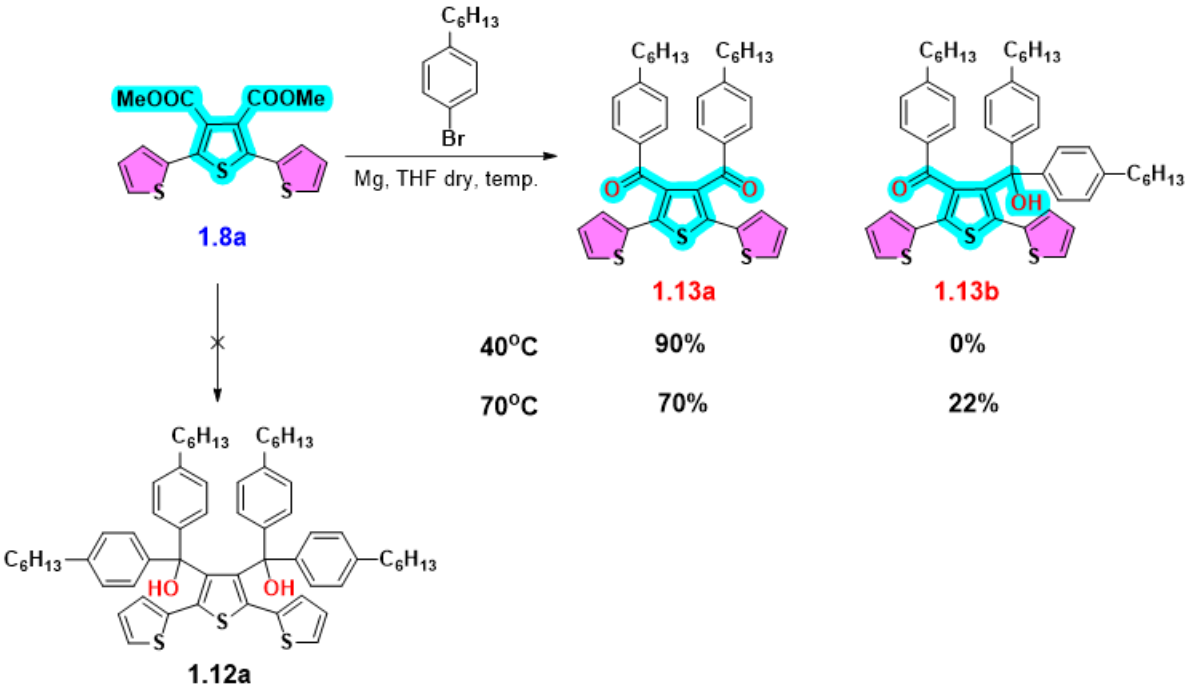

Scheme 1.3 Synthesis of diketone **1.13a**

Compound **1.8c** was designed and synthesized in order to bypass this issue by placing the ester moieties on marginal thiophenes. Indeed, the Grignard reaction of this isomer, under the same conditions as above, gave compound **1.12b** in very good yield of 76% (**Scheme 1.4**).

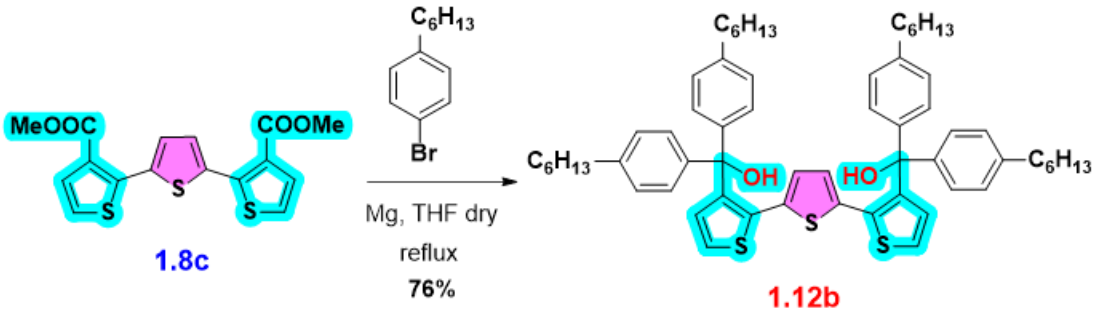

Scheme 1.4 Synthesis of diol **1.12b**

The cyclization reaction, catalyzed by *para*-toluenesulfonic acid (APTS) in dichloromethane, didn't produce the target compound, but compound **1.2b** in low yield, in which the central thiophene ring is broken and the naphtho[2,3-b]thiophene is being generate.

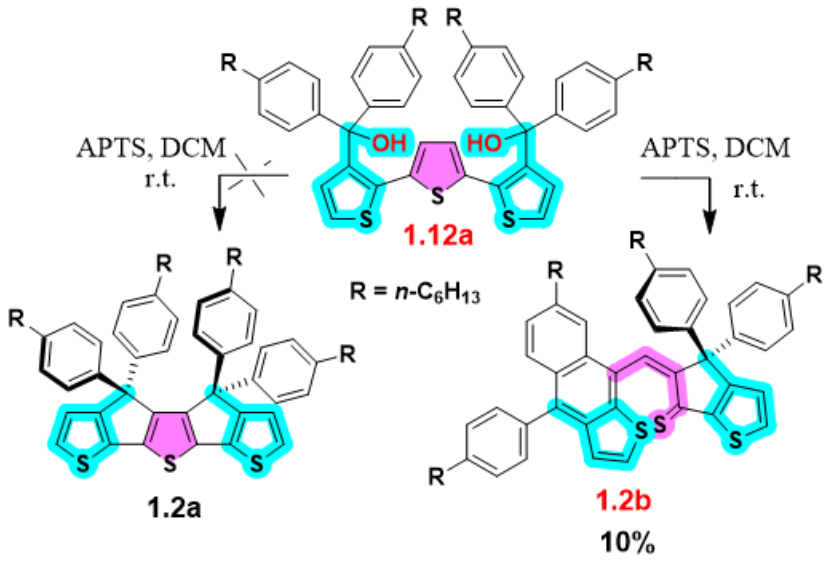

Scheme 1.5 Cyclization of **1.12a** by Friedel-Crafts intramolecular alkylation

1.2.2.2 Characterization of the naphtho[2,3-b]thiophene 1.2b

The structural identity of 1.2b was confirmed by NMR spectroscopy, X-ray diffraction and HRMS measurements. The compound 1.2b was also characterized by UV-VIS spectroscopy and cyclic voltammetry (CV), but the confirmation of the structure was of most importance.

Analysis of the 1D and 2D NMR spectra of compound **1.2b** was in agreement with the formation of a single diastereoisomer (**Figure 1.2a**), in which the double bond is in Z configuration with the bulky groups B/C and naphtho[2,3-*b*]thienyl placed on opposite sides. The proposed structure was confirmed by X-ray diffraction on single-crystal (**Figure 1.2 b**).

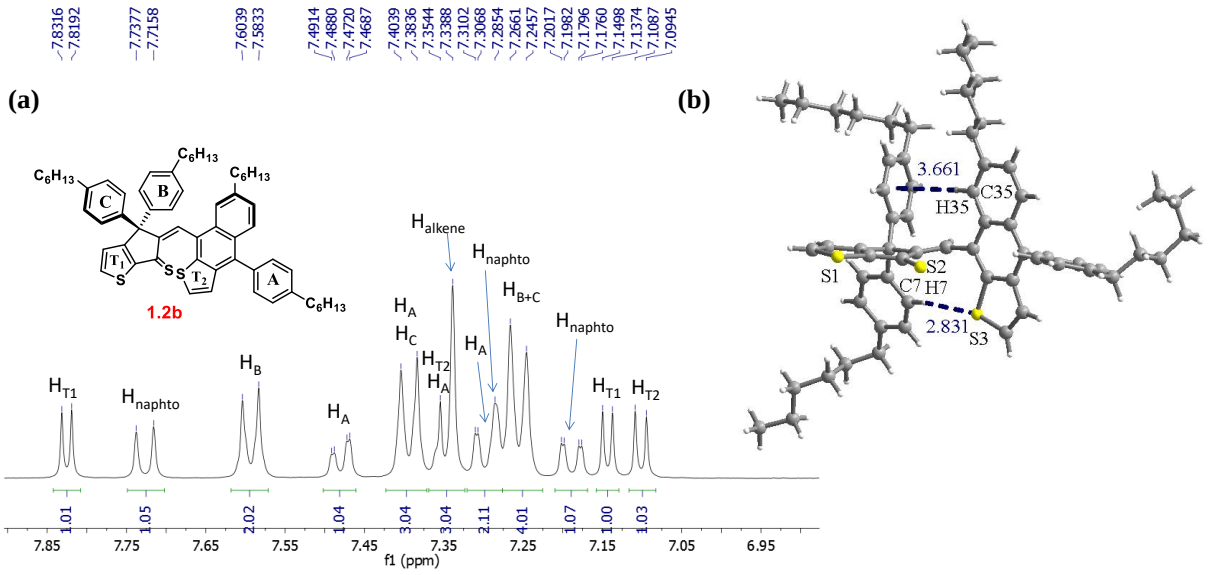

Figure 1.2 a) Fragment of ^{1}H-NMR spectrum of compound **1.2b** (DCM-d_2, 600 MHz, r.t.); b) Single-crystal molecular structure of compound **1.2b**

The observed reaction and the diastereotopicity of the phenyl A protons were also suported by Density Functional Theory (DFT) theoretical calculations.

1.2.3 Synthesis and characterization of new terthiophene and hexathiophene derivatives for OSCs

Starting from compound **1.8a** we have tried to obtain a new series of structurally simple NFAs with A-D-A-D-A structure. The low solubility of the target compound **1.3a** determined us to replace the methyl ester group with a more solubilizing alkyl, namely hexyl ester (**Scheme 1.6**). The 1.72% efficiency of the OSC fabricated from acceptor **1.3d** with P3HT motivated us to design the more extended structures **1.4a** and **1.4b** (**Scheme 1.7** and **Scheme 1.8**).

1.2.3.1 Synthesis of new terthiophene and hexathiophene derivatives for OSC

The synthesis of the terthiophene NFAs was performed by double formylation, followed by a condensation reaction with the appropriate nucleophiles (**Scheme 1.6**). The dialdehydes **1.14a** was obtained by a Vilsmeier-Hack reaction using high excess of $POCl_3$ and DMF (3 portions of 15 eq. each). Compound **1.14b** was generated by Rieche formylation, using a slight excess of $TiCl_4$ and dichloromethyl methyl ether (5 eq.). The acceptor groups used were malononitrile, 2-(3-oxo-2,3-dihydro-1H-1-inden-1-ylidene)malononitrile and *N*-ethylrhodanine.

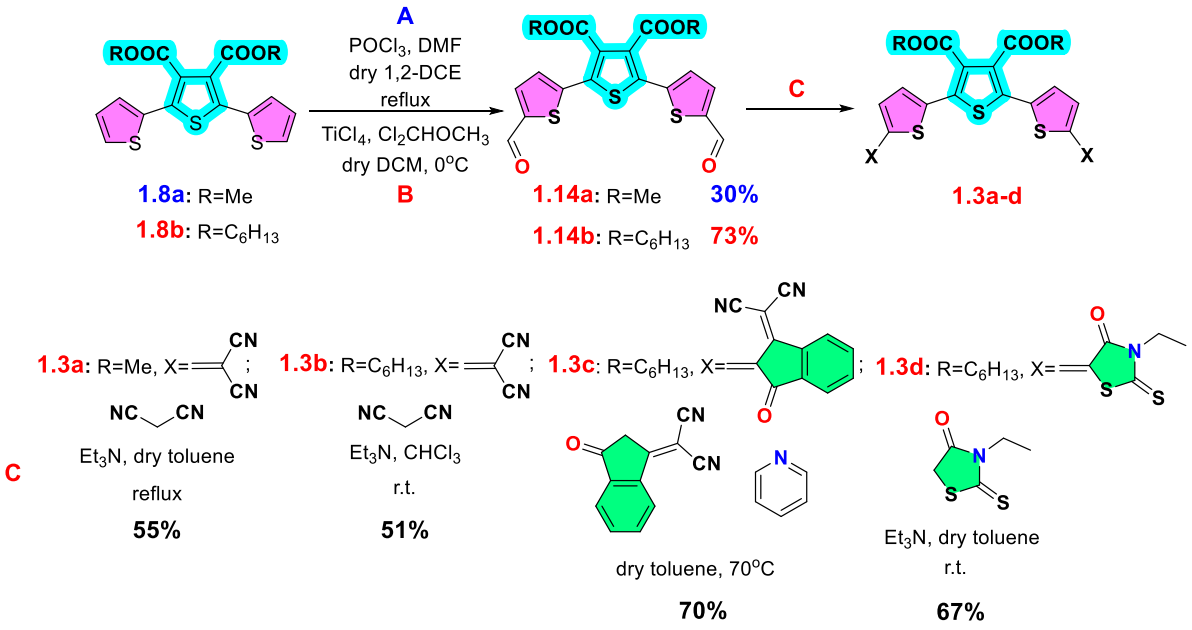

Scheme 1.6 Synthesis of terthiophene compounds **1.3**

Compound **1.4a** (**Scheme 1.7**) was also initially designed with methyl, but was later changed to hexyl due to the low solubility of the methyl compounds. The monoformylations of the terthiophene were performed similarly to the previous diformylation reactions, using a smaller exces. The dimerization reaction was a McMurry coupling catalyzed by $TiCl_4$ and Zn powder. The Vilsmeier-Haack formylation of **1.16a** was carried out using a very high excess (100 eq.) of $POCl_3$ and DMF to give dialdehyde **1.17** in 22% yield. This excess allowed for a shorter reaction time, *i.e.* 1 day over the 6 day time period used for the previously presented Vilsmeier-Haak formylations. The condensation with *N*-ethylrhodanine was realized in the same conditions as with **1.8b**.

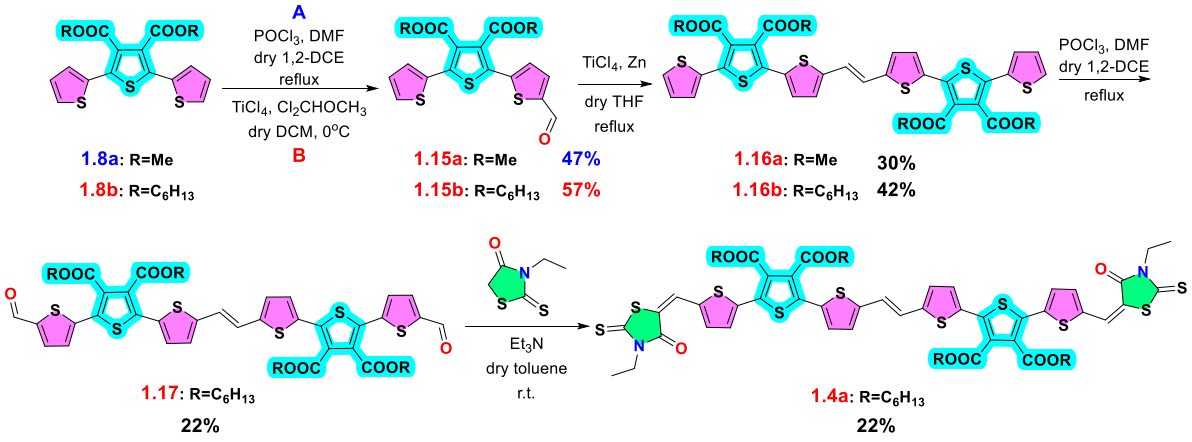

Scheme 1.7 Synthesis of hexathiophene NFA **1.4a**

Compound **1.4b** was obtained by a 4-step strategy: monobromination of **1.8b** with NBS, dimerization of **1.18** by Stille coupling reaction, formylation reaction (Vilsmeier-Haack/Reiche method) and condensation with N-ethylrhodanine (**Scheme 1.8**).

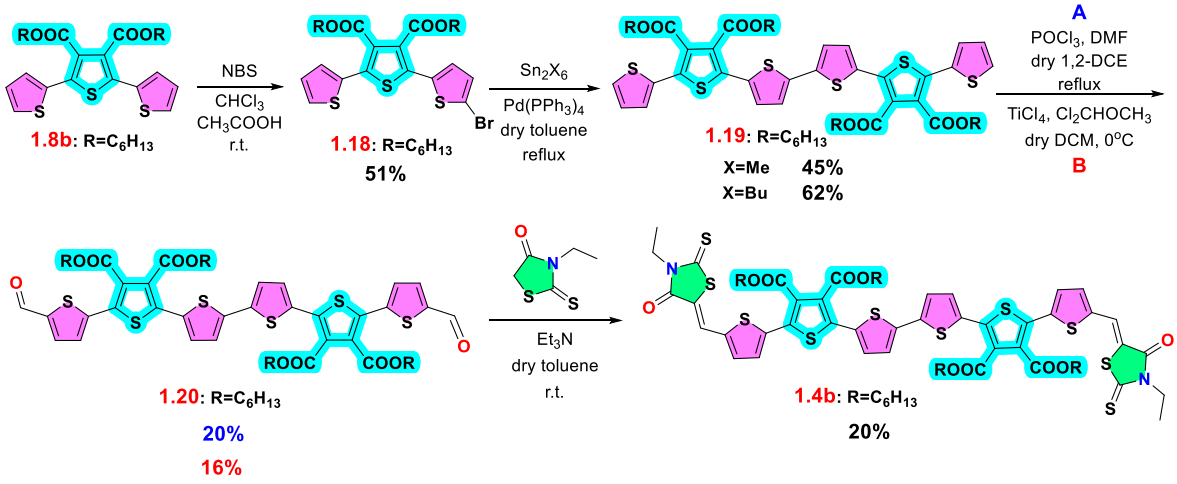

Scheme 1.8 Synthesis of hexathiophene NFA **1.4b**

1.2.3.2 Characterization of the terthiophene and hexathiophene derivatives

The synthesized compounds were characterized by NMR spectroscopy, HRMS, as well as UV-VIS spectroscopy and CV measurements. For a number of derivatives , the X-ray crystal structures were also determined (**1.14a**, **1.16a**, **1.3a**, **1.3b** and **1.3d**).

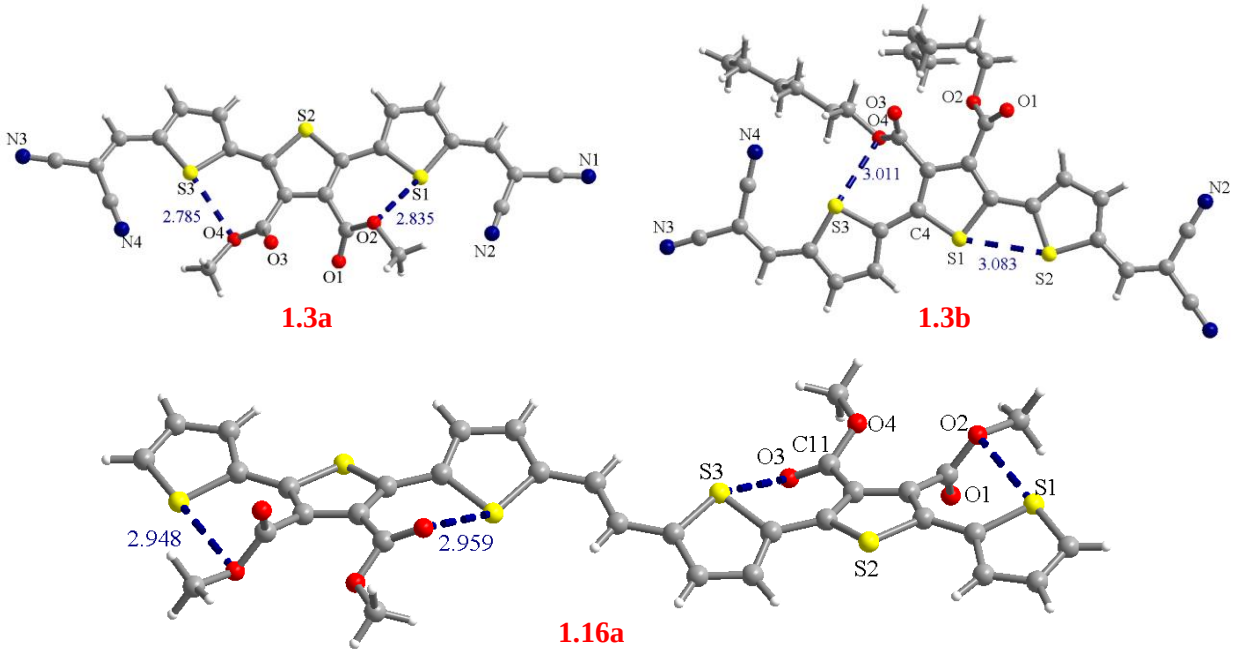

Figure 1.3 Crystal structure of derivatives **1.3a**, **1.3b** and **1.16a**

The X-ray structure of **1.16a** confirms the formation of the Z isomer. Also, the replacement of methyl with hexyl produced an important change in the conformation of the malononitrile derivatives **1.3b** and **1.3d**. A marginal thiophene flips and forms a S-S interactions with the central thiophene (**Figure 1.3**).

The malononitrile derivatives **1.3a** and **1.3b** present similar UV-VIS absorption spectra, with λ_{max} at 442nm and 435nm, respectively. Indandione proves to be the most efficient acceptor group, compound **1.3c** displaying a 64nm redshift to 532 nm compared to the N-ethylrhodanine derivative **1.3d** with λ_{max} of 468 nm. The increase in the number of thiophene rings resulted in a neglijible change of λ_{max}.

The CV measurements showed that compound **1.3d** present the highest HOMO among the terthiophene derivatives, with the oxidation peak at 1.45 V, and LUMO, with the reduction peak at -1.03V. Compound **1.3c** would have been the most suited terthiophene acceptor based on UV-VIS spectroscopy, as well as reduction CV, having the lowest lying LUMO level at -4.24 eV. The CV measurements showed an improvement in the bandgap of the hexathiophene derivatives, from 2.20eV for **1.3d** to 1.91eV for **1.4a-b** (**Table 1.1**). This difference is however caused by higher energy HOMO levels which correspond to lower oxidation potentials, and not by an improvement of the reduction potentials.

Table 1.1 UV-VIS spectroscopy (DCM) and cyclic voltammetry (0.10 M n-Bu_4NPF_6, DCM/MeCN, Pt electrodes, scan rate = 100 mV s^{-1}, ref SCE)

Compound	λ_{max} [nm]	ε_{max} [$M^{-1}\cdot cm^{-1}$]	E_g [eV][a]	ΔE [eV][b]	E_{pa}[V]	E_{pc}[V]	E_{HOMO}[c] [eV]	E_{LUMO}[c] [eV]
1.3a	442	$4.43\cdot10^4$	2.36	2.25	1.71	-0.82	-6.20	-3.95
1.3b	435	$4.65\cdot10^4$	2.39	2.23	1.79	-0.79	-6.30	-4.07
1.3c	532	$6.04\cdot10^4$	1.96	-	-	-0.55	-6.20[d]	-4.24
1.3d	468	$6.09\cdot10^4$	2.24	2.20	1.45	-1.03	-5.98	-3.78
1.4a	472	$8.35\cdot10^4$	2.16	1.91	1.10	-1.09	-5.65	-3.76
1.4b	463	$7.12\cdot10^4$	2.21	1.91	1.23	-1.08	-5.8	-3.76

[a]Calculated as 1.24/ λ_{max} offset (μm) [eV] [b]Calculated as $E_{HOMO}-E_{LUMO}$
[c]Using $E°_{ox}$ with an offset of −4.68eV for SCE vs the vacuum level [d]Calculated as $E_{LUMO}-E_g$

1.2.3.3 Application of the target compounds in OPV devices

The synthesized compounds were used as NFA acceptors in OSCs with P3HT as polymer donor using an inverted BHJ architecture ITO/ZnO/Organic Material/MoO_3/Al. The methyl diester **1.3a** could not be tested as NFA because of its lower solubility. The tests performed with compounds **1.3b** and **1.3c** gave very poor results. The results of the indanedione derivative can be explained by its tendency to form microcrystals instead of thin films. Compound **1.3d** gave the best results with P3HT when it was thermal annealed at 120°C, showing a 1.72% PCE.

The hexathiophene derivatives gave smaller efficiencies with P3HT, even after optimization, compound **1.4a** affording 0.38% efficiency and compound **1.4b** a better efficiency of 0.88%.

1.2.4 Synthesis and characterization of new D-A compounds for single material organic solar cells (SMOSCs)

The last part of this chapter shortly discusses the properties of some triphenylamine based molecules, as well as their application in the fabrication of single-material solar cells (SMOSCs).

The synthesis of **1.21**, **1.5a**[5] and **1.5b**[6] was performed according to the literature (**Scheme 1.9**). Both reactions took place in a moderate yield of 63% and 70% respectively. It can be observed that pyridine acts as a very good catalyst in Knoevenagel condensations of 2-(3-oxo-2,3-dihydro-1H-1-inden-1-ylidene)malononitrile.

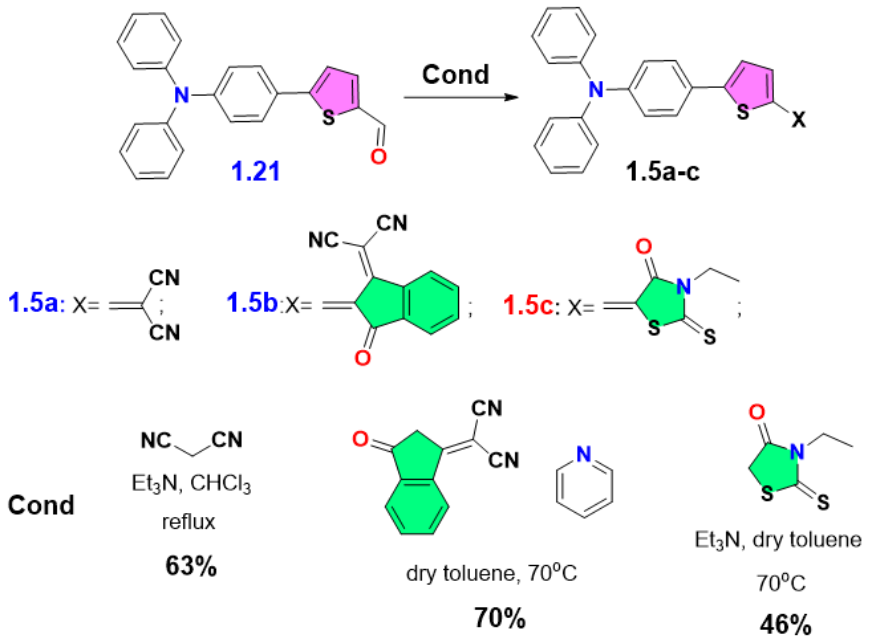

Scheme 1.9 Synthesis of the D-A compounds **1.5** from the aldehyde **1.21**

During purification, crystals suited for x-ray diffraction were obtained for compound **1.5c** (**Figure 1.4**). The crystal structure showed that the thiophene is basically coplanar with the *N*-ethylrhodanine moiety, the angle between the mean planes of the rings (Φ_2) is around 4.75°. This structure is also favored by a S-S interaction, S1···S2 distance of 3.265Å, smaller than 3.6 Å, the sum of their van der Waals radii. The other angle between phenyl and thiophene (Φ_1) is very large 31.90°, basically the largest for any compound of this series.

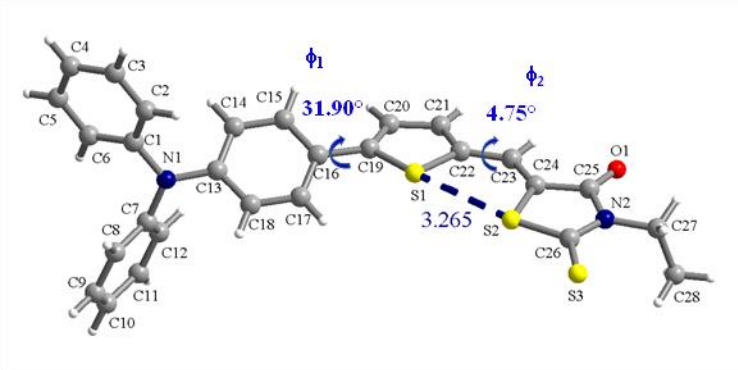

Figure 1.4 Crystal structure of compound **1.5c**

The UV-VIS absorbtion spectra of compounds **1.5a-c** display bands corresponding to π-π* transitions under 400nm for **1.5a** and **1.5c** and at 420nm for **1.5b**, as well as CT bands between the triarylamine (donor) and the acceptor groups at higher wavelengths. With malononitrile and *N*-ethylrhodanine the bands are situated around the same value, but 2-(3-oxo-2,3-dihydro-1H-1-inden-1-ylidene)malononitrile red shifts this band by around 100nm. This shift corresponds to a very small E_g bandgap (**Table 1.2**). The optical behavior of the compounds can be corroborated with their electronic properties obtained by CV measurements. The bandgaps calculated from the HOMO and LUMO levels, which were in turn calculated from the CV, present about the same 0.4 eV difference (**Table 1.2**) between **1.5b** and **1.5a**/**1.5c**.

Table 1.2 UV-VIS spectroscopy (DCM) and cyclic voltammetry (0.10 M n-Bu_4NPF_6, DCM, Pt electrodes, scan rate = 100 mV $s^{-1,}$ ref SCE).

Compound	λ_{max}[nm]	ε_{max} [$M^{-1}\cdot cm^{-1}$]	E_g [eV][a]	ΔE [eV][b]	E_{pa}[V]	E_{pc}[V]	E_{HOMO}[c] [eV]	E_{LUMO}[c] [eV]
1.5a	499	$4.01\cdot10^4$	2.16	1.91	1.06	-1.23	-5.60	-3.69
1.5b	602	$4.95\cdot10^4$	1.78	1.55	1.00	-0.79	-5.55	-4.00
1.5c	497	$4.36\cdot10^4$	2.13	1.92	0.96	-1.24	-5.50	-3.58

[a]Calculated as 1.24/ λ_{max}offset(μm) [eV]. [b]Calculated as E_{HOMO}-E_{LUMO}.
[c]Using $E°_{ox}$ with an offset of -4.68eV for SCE vs the vacuum level.

These D-A dyads were used as donor/acceptors and single materials in inverted OSCs with the architecture ITO/ZnO/Organic Material/MoO_3/Al. The OSCs efficiencies obtained so far from our experiments gave **1.5b** as the better single material with a 0.86% PCE, in concordance with the optoelectronic properties presented above (**Table 1.5**).. While **1.5a** displays a 0.55% efficiency, **1.5c** barely produces any electric current when it is irradiated.

These results could be in turn corroborated with the X-ray data. The Φ_1 and Φ_2 angles between the mean planes of thiophene and triphenyl amine, and thiophene and the acceptor moiety, respectively, are higher for **1.5c** than for **1.5a**. This shows that the effective conjugation is better in the case of **1.5a** compared to **1.5c**.

1.3 Conclusions

In conclusion we have attempted the synthesis of a new rigidified terthiophene based NFA. We have observed the unexpected formation of a naphto[2,3-thiophene] derivative 1.2b, which was fully characterized by X-ray diffraction on single crystal, NMR spectroscopy, HRMS, UV-VIS absorption spectra and CV measurements. Our experimental results were also confirmed by theoretical DFT calculations.

We have also synthesized and characterized a new series of terthiophene diesters and hexathiophene tetraesters. Initially the compounds were designed with methyl ester, but the low solubility of compound **1.3a** led to the hexyl target compounds **1.3b-d**. The poor efficiencies of **1.3b** and **1.3c** OSCs, and 1.72% PCE of **1.3d** OSC lead to the design of **1.4a** and **1.4b**. Despite and improvement of the electronical bandgap the hexathiophene derivatives gave poorer results.

The last part of the chapter presented contributions in the synthesis and characterization of some D-A triarylamine donors, which were used as single materials for OSC with very good results. The PCE of the SMOSCs is influenced by the optical properties of the material, as well as by the degree of conjugation, but the mechanism is still up for debate. While a clear understanding of the functioning of this type of material is still to be formulated, we believe that our results are an important stepping stone towards it.

Chapter 2. Synthesis and characterization of new ESPT and ESIPT 2,5-disubstitued-1,3,4-oxadiazoles

2.1 Introduction

From the point of view of sustainable environmental development, besides the great interest for new materials able to convert solar energy into electrical energy (see chapter I), unraveling new materials or technology for energy-efficient lightening products is current scientific concern. In this context we were interested in a class of compounds, namely 2,5-disubstituted-1,3,4-oxadiazoles (**Figure 2.2**), which have been known for their applications as electron transport materials in organic light emitting diodes (OLEDs). These devices are designed to do the opposite of solar cells and turn electrical energy into light, in our homes, with very energy-efficient manner. Our target compounds are decorated with phenol groups which led to them presenting Excited State Intramolecular Proton Transfer (ESIPT) or Excited State Intermolecular Proton Transfer (ESPT).

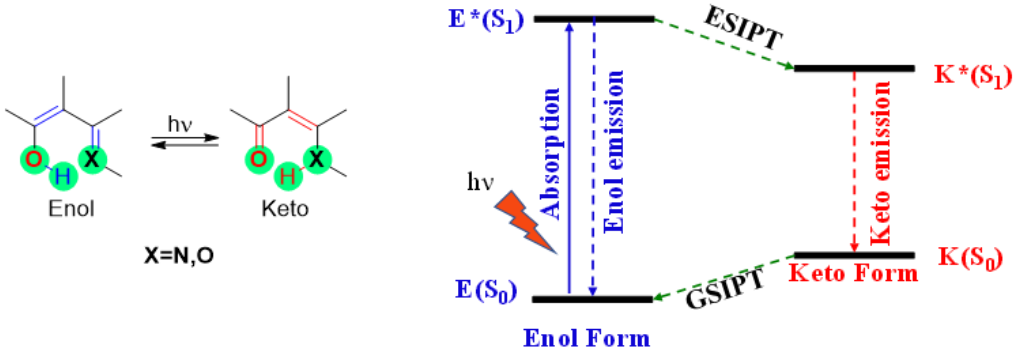

Figure 2.1 Schematic description of ESIPT process

ESIPT process usually occurs in compounds that able to form stable intramolecular hydrogen bonds in a five- or six-membered ring between a donor group (*i.e.*, OH, NH_2) and an acceptor group (*i.e.*, C=O, C=N), thus making possible the tautomerization process. It can also be observed from the Jablonski diagram (**Figure 2.1**) that besides the normal enol emission, at lower wavelengths, a second emission is generated at a larger wavelength by the keto form.

2.2 Results and discussion

This chapter is focused on two directions of research into hydroxy decorated 2,5-disubstituted-1,3,4-oxadiazoles, which display interesting optical properties, excited state proton

transfer, either intramolecularly (ESIPT) or intermolecularly (ESPT) (**Figure 2.2**). The first series of compounds **2.1** and **2.2**, continues our efforts into developing new ligands for metal-ion coordination,[7] by adding good coordinating functional groups as hydroxy or groups which can be further functionalized like formyl for compounds **2.2**. The formylated compounds can be regarded as oxadiazole functionalized salicyladehyde (**2.2a**) and *o*-vanilin (**2.2b**). The synthesis and structural characterization of the compounds were performed during my master studies.

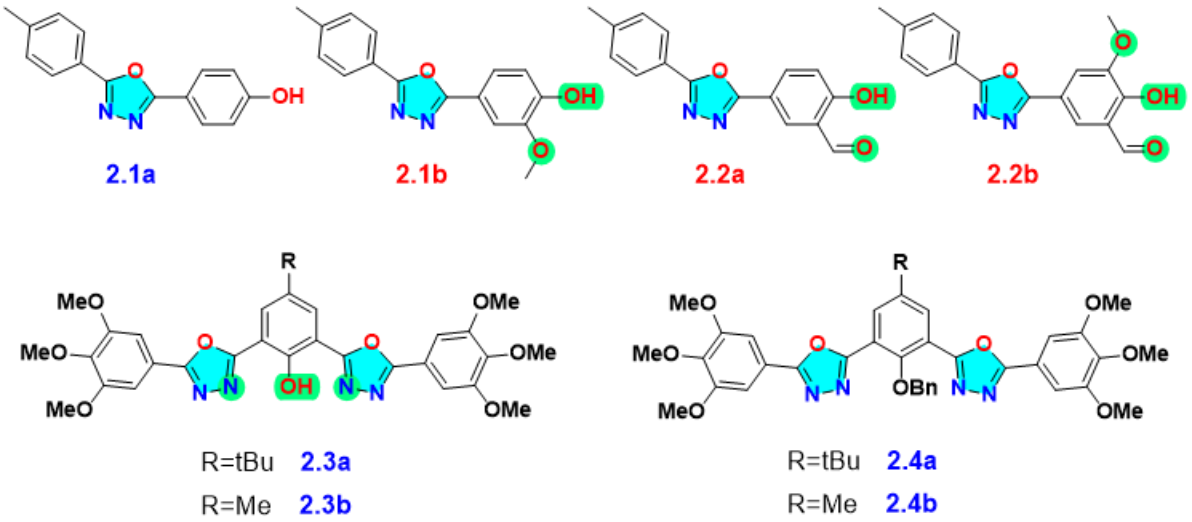

Figure 2.2 The structure of the oxadiazole discussed in first subchapter **(2.1** and **2.2)** and the second subchapter **(2.3** and **2.4)**

2.2.1 The synthesis and characterization of compounds 2.1 and 2.2

2.2.1.1 The synthesis of compounds

To combine the oxadiazole motif with salicylaldehyde or *o*-vanillin residues, the synthetic strategy we firstly approached involved the construction of the oxadiazole ring (**Scheme 2.3**), which required *p*-tolyl hydrazide and the corresponding phenol aldehydes. The method of choice for the preparation of the heterocyclic ring was the oxidative cyclisation of the *N*-acylhydrazones **2.6a,b** and having known the susceptibility of the phenols to oxidative agents like hypervalent iodine reagents,[8] we used benzyl-protected aldehydes **2.5a,b**. that after treatment with either stoichiometric amounts of bis(trifluoroacetoxy)iodobenzene (PIFA)[9] or molecular iodine, under basic conditions[10] provided oxadiazoles **2.7a,b** in very good to excellent yields (70%-92%). Further, the benzyl group was removed either by hydrogenolysis or under action of HBr (33% wt in AcOH), to yield compounds **2.1a,b** which were subsequently subjected

to Duff conditions (trifluoroacetic acid and hexamethylenetetramine) to achieve aldehydes **2.2a** in 56% yield and **2.2b** in 76% yield.

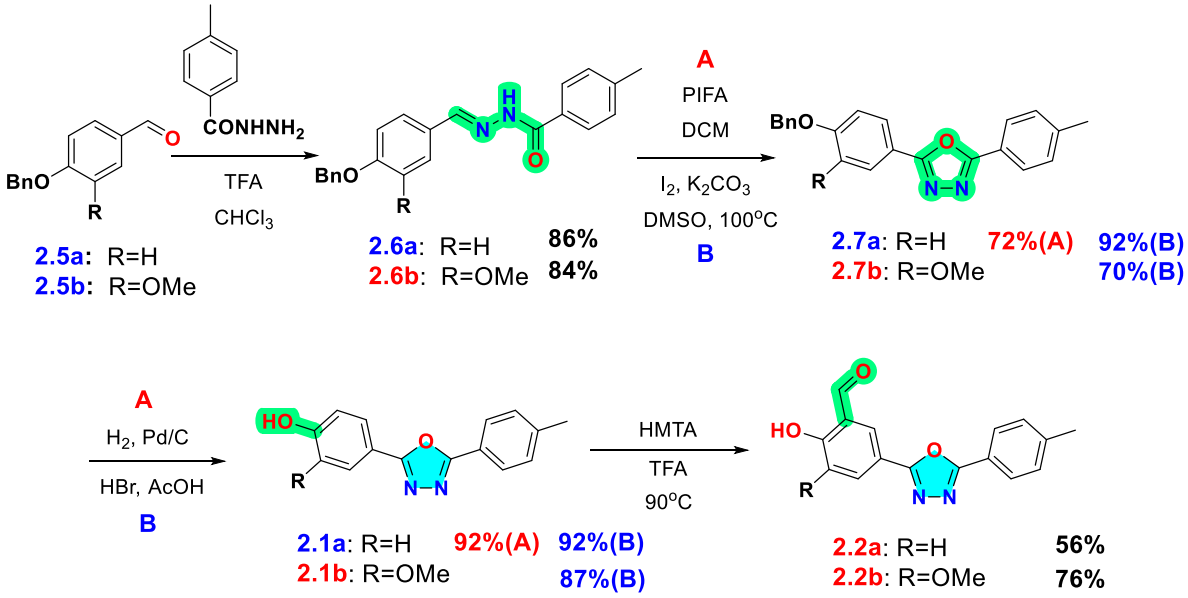

Scheme 2.1 Synthesis of the target compounds **2.1** and **2.2**

2.2.1.2 Structural and optical properties characterization

All compounds were structurally characterized to confirm their identity by NMR and HRMS. Ability of some compounds to form inter- or intramolecular hydrogen bonds in solution has also been investigated by NMR.

The signal corresponding to O***H*** groups of compounds **2.1a**, **2.1b**, **2.2a** and **2.2b** in DMSO-d_6 appear in a distinct region of δ=9.94–11.55 ppm (**Figure 2.10**). The +E electromeric effect of the methoxy group can be observed from the shielding of the OH proton, from δ=11.55 ppm for **2.2a** to δ=11.05 ppm for **2.2b**, from δ=10.37 ppm for **2.1a** to δ=9.94 ppm for **2.1b**.

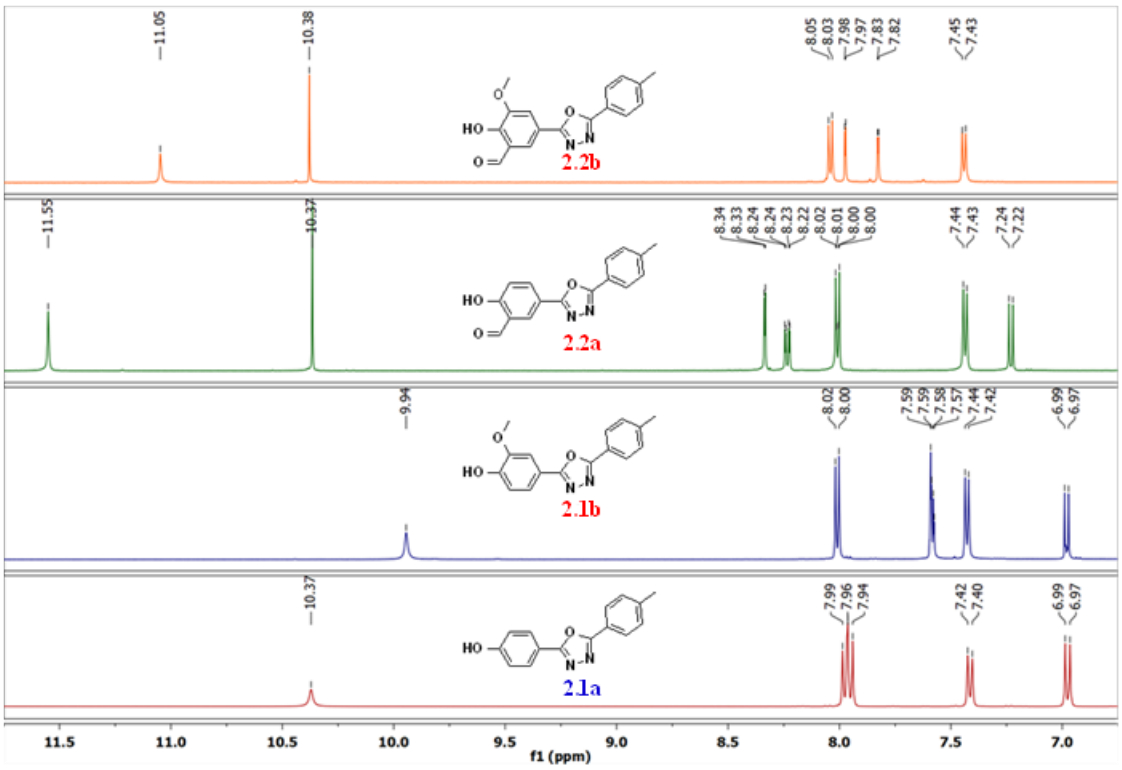

Figure 2.3 ^{1}H-NMR spectra of compound **2.1a**, **2.1b**, **2.2a** and **2.2b** in DMSO-d_6 (500 MHz)

The molecular structures of compounds **2.1a**, **2.1b**, **2.2a** and **2.2b** (**Figure 2.4**) were obtained by X-ray diffraction on single crystals. First observation was that compounds **2.1b**, **2.2a** and **2.2b**, which possess oxygen containing functional groups nearby the phenol group, present intramolecular hydrogen interactions. All compounds are basically planar (with angles between the mean planes of the 1,3,4-oxadiazole and the adjacent aryl rings below 6°), except for **2.1a** where the angles between the mean planes of the rings are 7.7° (oxadiazole - tolyl) and 19.7° (oxadiazole - phenol). The analysis of the packing diagrams for compounds **2.1a**, **2.1b**, **2.2b** showed formation of supramolecular chains through hydrogen bond interactions established between the phenol group and a nitrogen atom of the oxadiazole ring belonging to a neighboring molecule. Compounds **2.1b** and **2.2b** are involved in bifurcated hydrogen bonding interactions because of the intramolecular hydrogen interactions. Packing of the molecules in crystal **2.2a** followed a different pattern driven mainly by π–π interactions.

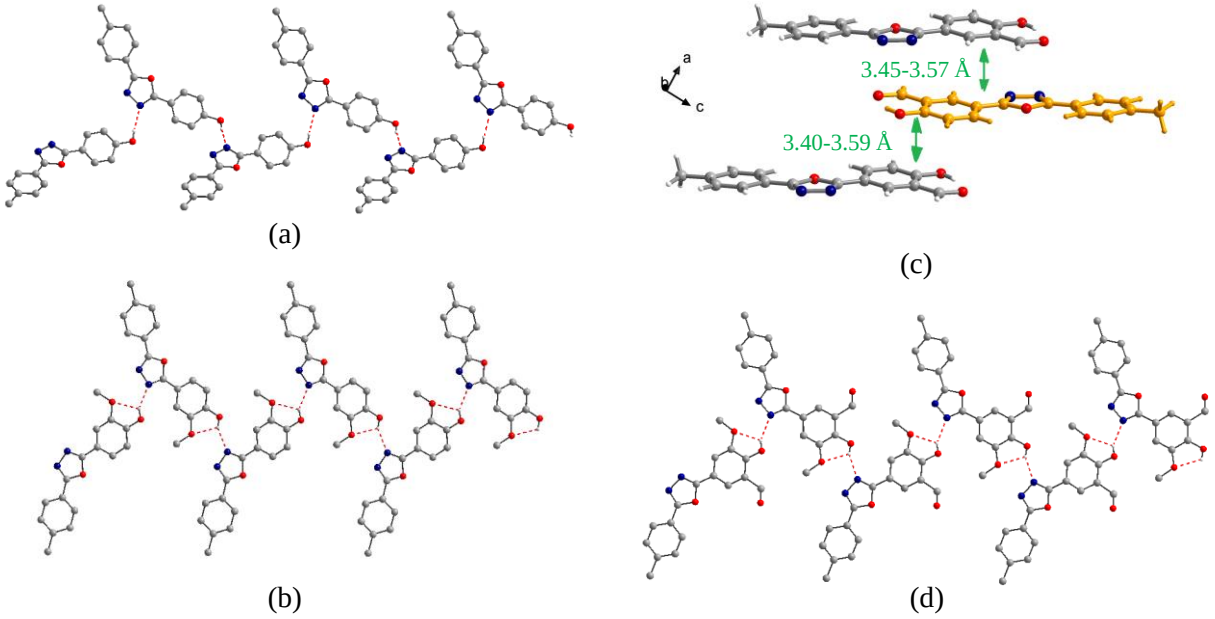

Figure 2.4 View of the supramolecular chains created by hydrogen interactions of compounds**: a)** 2.1a**; b)** 2.1b**; d)** 2.2b**;** π−π interactions shown by **c)** 2.2a

Nest we investigated the absorption and emission properties of the synthesized compounds in solution using $CHCl_3$, MeCN, MeOH and DMSO as solvents. The UV-Vis spectra indicated slight changes in profiles depending on the solvent, with absorption maxima ranging between λ_{max}=291 nm and λ_{max}=314 nm, assigned to the characteristic π-π* transitions of the oxadiazole core, as previously observed,[11] as well as small shoulder bands around λ_{max}=330 nm for **2.2a** and around λ_{max}=370 nm for **2.2b**.

The emission spectra are displayed in **Figure 2.5**. At first glance, a few general distinctive features could be observed: compounds **2.1a,b** display a higher emission intensity than compounds **2.2a,b** in all solvents, except methanol, and, notably, the highest emission intensity occurred in DMSO for **2.1a**. The emission maxima are similar for $CHCl_3$, MeCN, MeOH and significantly different when DMSO was used as solvent.

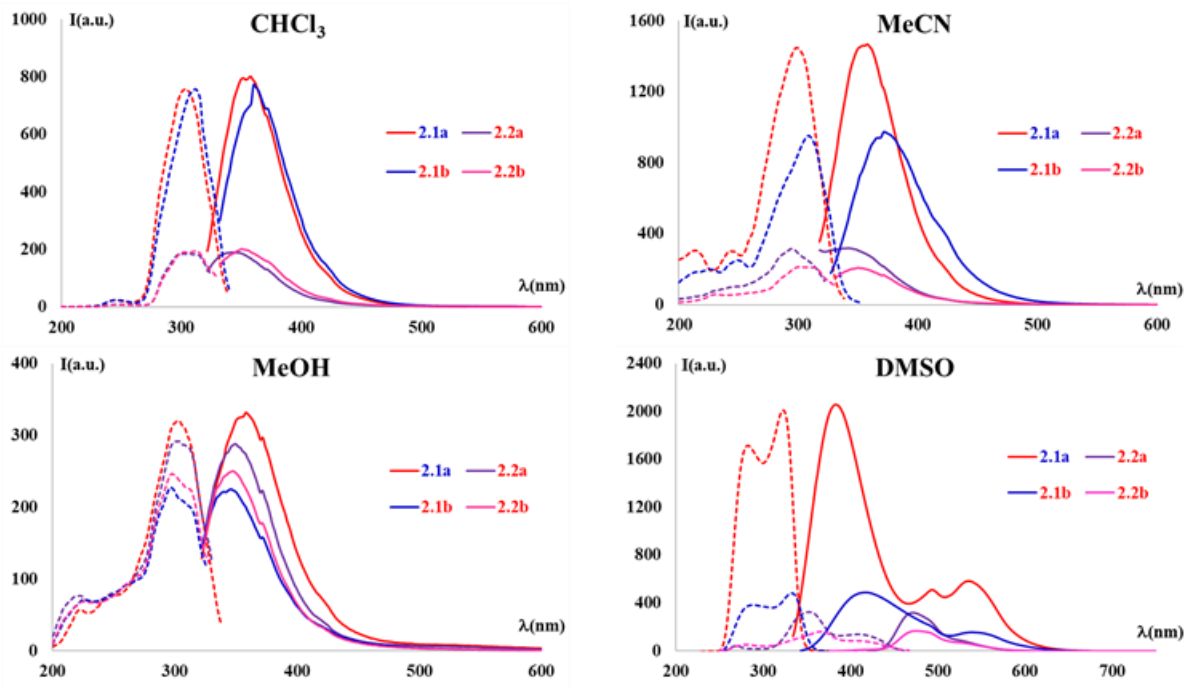

Figure 2.5 Excitation and emission spectra of compounds **2.1a,b** and **2.2a,b** in solution (performed at 5·10-5 M)

Compound **2.1a** underwent a redshift in the emission wavelength of almost 25 nm by changing from less polar solvents (λ_{em}=358-359 nm) to DMSO (λ_{em}=383 nm) concomitant with appearance of two new emission bands at λ_{em}=494 nm and λ_{em}=535 nm. While the emission at lower wavelength could be assigned for typical behavior of oxadiazole-based compounds,[12,13] the emissions at longer wavelengths was probably due to the presence of the hydroxyl group which allows intermolecular hydrogen bonding or with polar solvents (*i.e.* DMSO) and further, a tautomerization process involving the oxadiazole core could occur. As far as the longest band (λ_{em}=535 nm) was concerned, this could arise either from aggregation[14] or as results of H bonding interaction with DMSO molecules. Compound **2.1b** underwent even more significant redshift when DMSO was used as solvent (λ_{em}=417 nm) and lower intensity emission bands above 500 nm were also visible. Addition of a methoxy group on the oxadiazole structure afforded both intra- and intermolecular hydrogen bonding and, therefore, multiple species in the excited state. Compound **2.1b** also displayed a band caused by aggregation and/or interaction H-bond interaction **2.1b** - DMSO at λ_{em}=540 nm.

To support behavior of the compounds in solvents of different polarity as most likely affected by intra and intermolecular interactions, the corresponding benzyl-protected compound

2.7b was also investigated (**Figure 2.6**), and the spectra indicated only one very intense emission band in DMSO, at λ_{em}=391 nm, confirming the effect of the hydrogen bonding interactions.

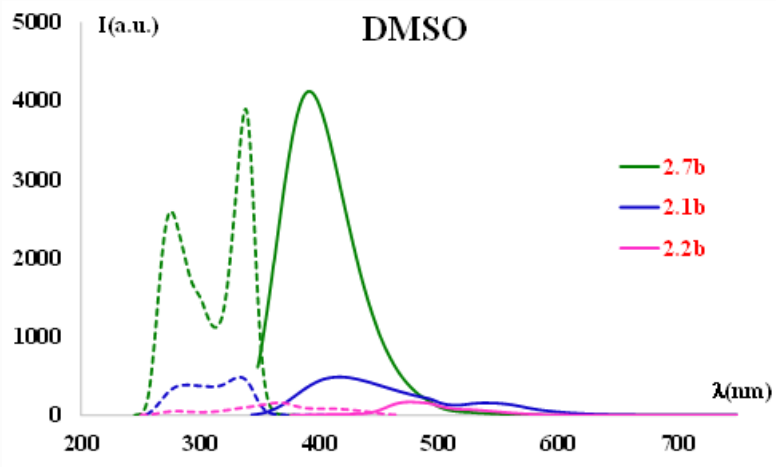

Figure 2.6 Excitation (dotted lines) and emission (plain lines) spectra of **2.7b, 2.1b** and **2.2b** in DMSO (50 μM)

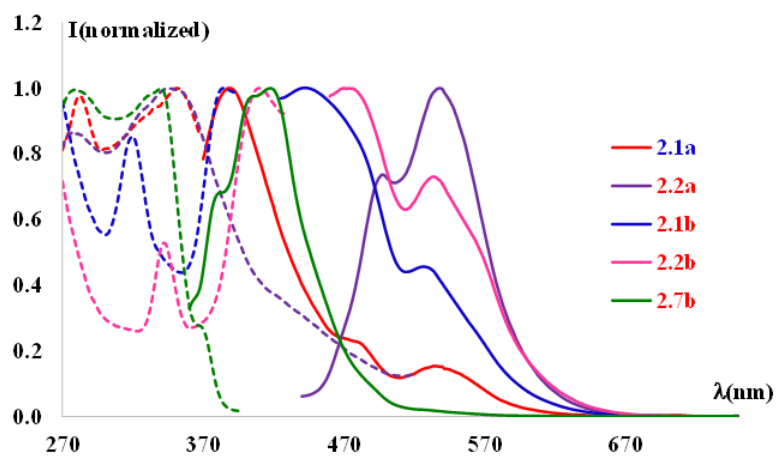

Figure 2.7 Excitation and emission spectra of compounds **2.1a,b** and **2.2a,b** and **2.7b** in solid state (in KBr)

In solid state, we could observe a change in the emitted light from blue to green. For example, the fluorescence spectra of compounds **2.1b**, **2.1b** and **2.2b** indicated a redshift in the absorption maxima. While the benzylated compound exhibited one emission band, at λ_{em}=420 nm, compounds **2.1b** and **2.2b** displayed two emission bands: at λ_{em}=438 nm for **2.1b** and λ_{em}=470 nm for **2.2b** and a less intense longer wavelength band, at λ_{em}~530 nm. Similar to the spectra in DMSO solutions, the shorter wavelength maxima could be assigned to intramolecular proton transfer and tautomerisation process in the excited state, under irradiation, while the longer wavelength maxima could be assigned to aggregation. The quantum yields underwent

drastically decrease from the benzylated compound **2.7b** to the hydroxy **2.1b** and formyl-derivative **2.2b**. The quantum yields for the target compounds were all under 2%.

2.2.1.3 Synthesis and characterization of cocrystals

Organic co-crystals are very attractive multicomponent materials[15] due to the new properties brought by the huge variety of molecular building blocks that can be used and the non-covalent interactions established between the individual components.

In our co-crystallization experiments we intended to take advantage of two type of non-covalent interactions: hydrogen bonding, electrostatic and π–π interactions. For this reason, we used as partners for compounds **2.1a**, **2.1b**, **2.2a** and **2.2b** different pyridyl derivatives: 2,5-bis(4-pyridyl)-1,3,4-oxadiazole; 4,4'-bipyridyl; *trans*-1,2-bis(4-pyridyl)ethylene. In the presence of phenol derivatives, the pyridyl moieties can act as hydrogen bond acceptor generating co-crystals or as proton acceptor forming organic salts.[16]

Three types of co-crystals were obtained by slow evaporation, at room temperature, from mixtures of EtOH and $CHCl_3$ using 1:1 or 2:1 stoichiometries between the components. From **2.1a** and 2,5-bis(4-pyridyl)-1,3,4-oxadiazole (4-bpo) in 1:1 molar ratio was obtained the co-crystal A (**CoA**). For 2:1 molar ratio between **2.1b** and 4,4'-bipyridyl (bipy) and **2.2b** with *trans*-1,2-bis(4-pyridyl)ethylene (bpete) the co-crystal B (**CoB**), and the co-crystal C (**CoC**) (**Figure 2.27**).

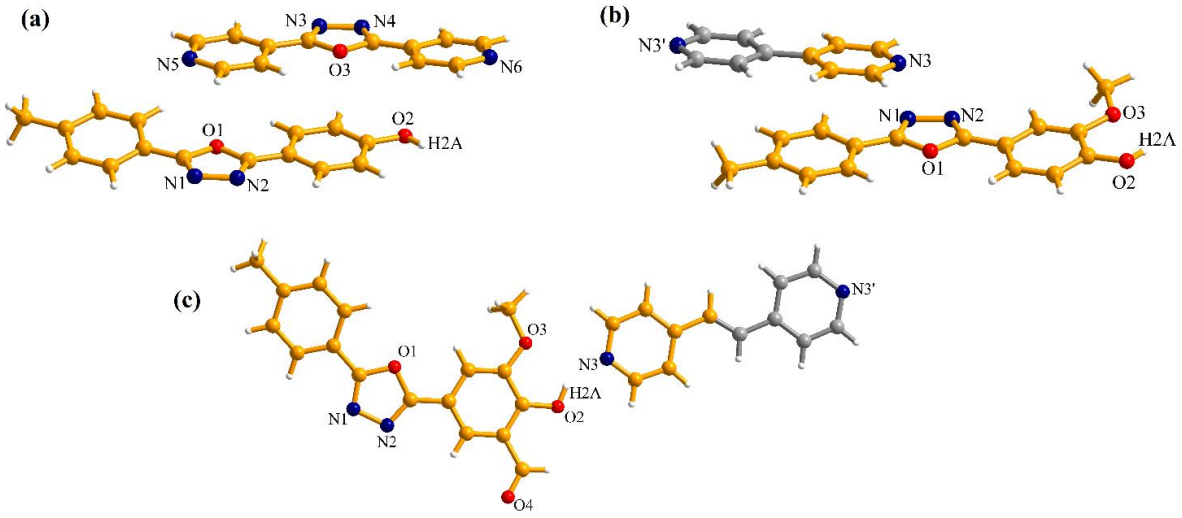

Figure 2.8 Molecular structures of co-crystals **CoA (a), CoB (b)** and **CoC (c).** The asymmetric units are labelled in orange.

2.2.2 Characterization of optical properties of bisoxadiazoles

The second subchapter covers the characterization of ESIPT photophysical properties of bisoxadiazoles **2.3** (**Figure 2.9**). During the study of the electronic and optical properties, we took into consideration our previous findings[17] of related compounds, precursors of our target compounds **2.3**, namely the corresponding bis-*N*-acylhydazones, which we found to be photoresponsive. This occurs according to the environment, due to the possibility to display ESIPT, but also because of the aggregation triggered by solvent.

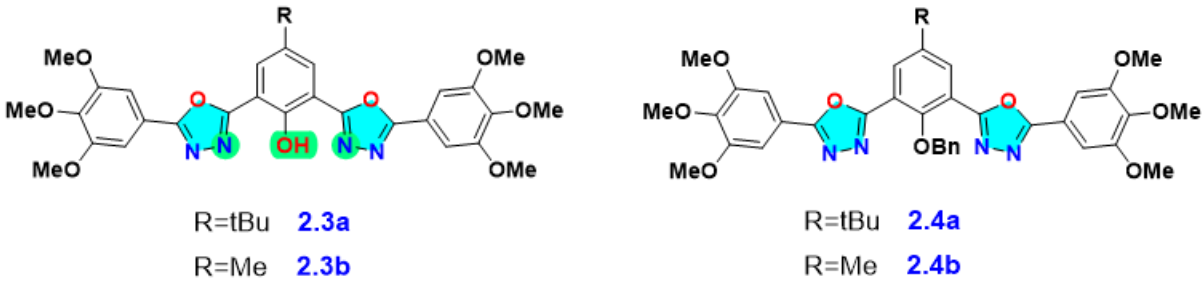

Figure 2.9 Structure of bisoxadiazoles **2.3** and **2.4**

Since ESIPT process is highly dependent on the solvent used, we performed our studies in solvents with different polarity: dichloromethane, DMSO and 10% DMSO/water. The excitation and emission spectra differ according to the protection of the hydroxyl group and the polarity of the solvent used (**Figure 2.10**). In dichloromethane, the spectra recorded at 5 x10^{-7} M display one clear emission band: green light for compounds **2.3** (λ_{em}=535 nm for **2.3a** and λ_{em}=538 nm for **2.3b**) and blue light for compounds **2.4** (λ_{em}=421 nm). These bands are accompanied by shoulders around λ_{em}=500 nm. The Stokes shifts are very large for compounds **2.3** (>15000 cm^{-1}) compared to previous reports for hydroxy-oxadiazoles (~12000 cm^{-1}).[18] Structure of compounds **2.3** indicates the possibility of ESIPT process occurrence between the phenol hydroxyl and one nitrogen atom of the oxadiazole core. The intense emission band is most likely due to the ketone tautomer resulted in the excited state by proton transfer in a higher amount, which occurs at longer wavelength, in the green region, while the shoulder at the shorter wavelength may be assigned to the emission from the enol tautomer. Emission in green region (λ_{em}~535 nm) is a notable difference of our compounds compared to most previous data which mainly report blue-shifted emissions (λ_{em}~500 nm[18]), with one exception, which involves two protons transfer and the emission is red-shift toward orange.[19]

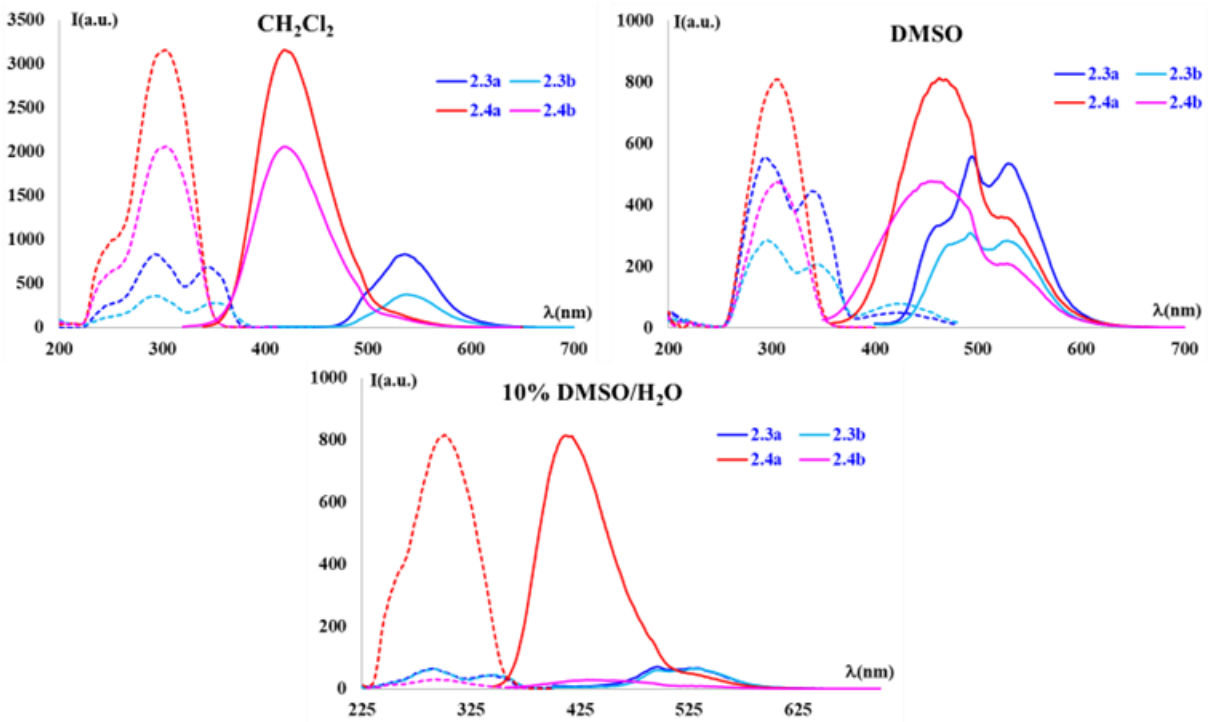

Figure 2.10 Excitation (dotted lines) and emission (plain lines) spectra of compounds **2.3** and **2.4** in DCM, DMSO and 10% DMSO/water (0,5 µM).

In solid state (dispersion in KBr), the emission spectra show green emission light for compounds **2.3** and blue emission light for compounds **2.4** (**Figure 2.11**). Compounds **2.3** display emission maxima at λ_{em}=545 nm, with a small shoulder at λ_{em}=500 nm, very clearly visible for **2.3b**, most likely due to the keto tautomer. The Stokes shifts for compounds **2.3** are large and comparable, as expected for compounds displaying ESIPT, even in solid state.[20] However, this is not valid in the case of the quantum yields, which are very different; compound **2.3a**, bearing a *t*-butyl group shows a very good quantum yield 54%, while determinations for **2.3b**, bearing a methyl group indicated almost a complete quench of the fluorescence.

The protected compounds **2.4** show intense emissions maxima around λ_{em}=410 nm, with a small shoulder around λ_{em}=480 nm and a band around λ_{em}=525 nm, with lower intensity. The Stokes shift are almost half the values corresponding to compounds **2.3**, suggesting the importance of the preformed hydrogen bond that enables the transfer of proton in the excited state. One can note the remarkable high quantum yields of these compounds with respect to previous reports, which confirm the properties the *t*-butyl provides, considering the quantum yield of **2.4b** is half of the value corresponding for **2.4a**, most likely due to intermolecular quenching effects.

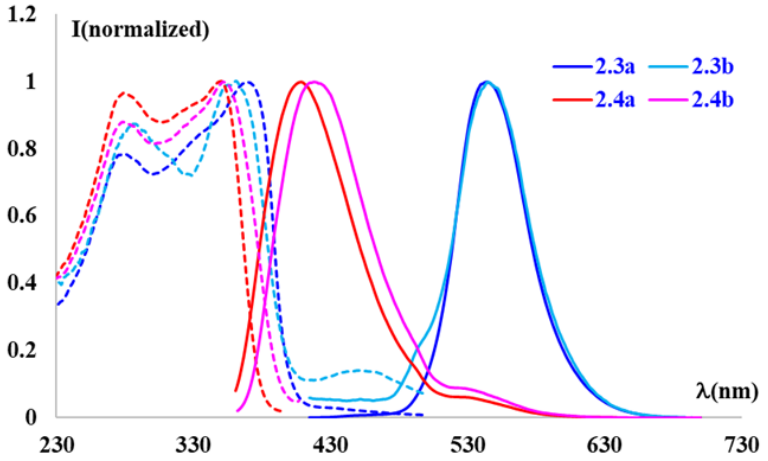

Figure 2.11 Solid state excitation (dotted lines) and emission (plain lines) normalized spectra of compounds **2.3** and **2.4** dispersed in KBr

2.3 Conclusions

In conclusion, the first part of the chapter described the synthesis of a new series of 1,3,4-oxadiazole-based compounds decorated with salicylaldehyde or o-vanillin residues and aimed to study their optical and electronic properties. The structures of compounds were fully characterized by NMR, HRMS and X-Ray diffraction experiments showing the occurrence of intra- and intermolecular hydrogen bonds interactions both in solution and solid state. Experimental and theoretical investigation of the absorption and emission behavior of the studied compounds indicated beside the characteristic optical properties of the 1,3,4-oxadiazole containing compounds, the influence of the solvent as well as of hydrogen bonding on the emission properties through ESIPT (for compounds **2.2a** and **2.2b**) and ESPT processes both in solution and in solid state. Moreover, the investigated compounds were successfully used in co-crystallization experiments with pyridine derivatives. Hydrogen bonding and π-π-stacking non-covalent interaction were found to be responsible for the supramolecular recognition between the two types of components of the co-crystals as inferred from single crystal X-ray diffraction experiments.

The second part of this chapter was focused on the investigation by UV-Vis and fluorescence spectroscopy bis-oxadiazoles **2.3** and **2.4**. Their spectra display emission maxima in the green region for the unprotected compounds and in the blue region for the protected compounds. While the blue light is common for the oxadiazoles, the green emission was

assigned to the proton transfer from the phenol to the nitrogen atom of one oxadiazole core when irradiated with light, through the ESIPT phenomenon. The spectra are different according to the polarity of the solvent used, indicating the possibility to modulate the emission. The optical parameters are remarkably different from previous reported data, with Stokes shifts higher than 15000 cm^{-1} and very high quantum yields. The structural particularities of the newly synthesized compounds do not allow intramolecular fluorescence quenching and the quantum yields are almost half of the value of the fluorescein standard for the green-emissive compounds (**2.3**) and almost equal to the value of the quinine, for the blue-emissive, benzyl-protected compounds (**2.4**). In solid state, compound **2.3a** is very luminescent compared to compound **2.3b**, proving the importance of tertbutyl instead of methyl as a substituent.

Chapter 3. Synthesis of new [2]rotaxanes by metal active CuAAC clipping

3.1 Introduction

[2]Rotaxanes are mechanically interlocked molecules (MIMs) comprised of two independent structures, which are not covalently bonded together, namely a dumbbell-shaped molecule, which is usually a linear chemical structure, known as axle, with bulky fragments at the extremities and a macrocycle threaded onto the axel (**Figure 3.1**).[21] The bulky fragments are referred to as stoppers and their role is to prevent the macrocycle from leaving the chemical ensemble.

Figure 3.1 The general structure of a [2]rotaxane

3.1.1 Synthetic strategies of [2]rotaxanes

The most important methods used in the synthesis of [2]rotaxanes are capping, clipping, metal active template and snapping, which is very similar to capping (**Figure 3.2**).[21–28] Other methods which can be used are shrinking,[29,30] swelling[31] and transition state stabilization,[32–34] the last one resembling metal active template.

The capping method requires initial preparation of a supramolecular structure called [2]pseudorotaxane, formed between a macrocycle and a linear shaped compound (the axle), which passes through the macrocycle. The synthesis is completed by the attachment of the stoppers. This method only allows the synthesis of symmetric [2]rotaxanes. Snapping on the other hand, while it similarly requires initial formation of a supramolecular structure, a [2]semirotaxane, *i.e.* the complex between the macrocycle and the axel that also contain at one of its ends the a stopper, generates unsymmetric compounds.

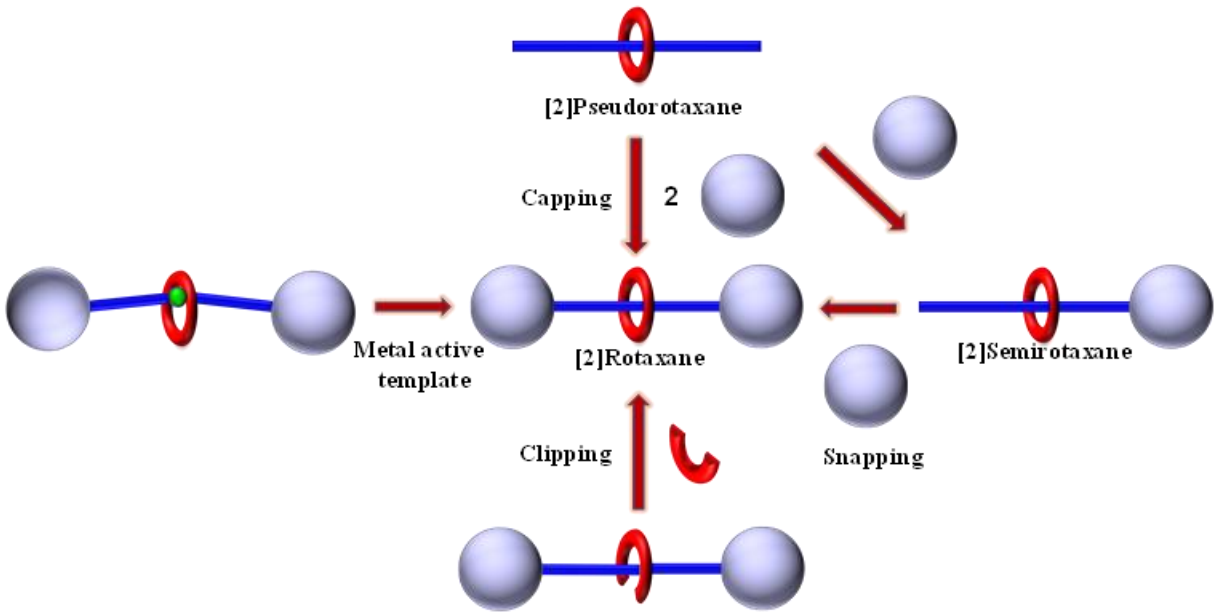

Figure 3.2 Synthetic strategies of [2]rotaxane

3.1.2 Applications of [2]rotaxanes

The [2]rotaxane literature is also rich when it comes to applications. Starting from the simplest molecular machine, the degenerate molecular shuttle *i.e.* molecular shuttle that have two identical recognition sites (stations), synthesized by Stoddart in 1991[35], the field of applications never stopped advancing. Numerous reviews summarize the development of molecular switches, where the position of the macrocycle on the axle can be controlled by applying various stimuli: addition of different ions,[36] pH modification,[37] light[38–40] or redox potential[41,42]. Also, thanks to their response to ions, [2] rotaxanes have been also described as sensors.[43]

3.1.3 Copper (I) N-heterocyclic carbenes (CuNHCs)

Carbenes have been known as a very unstable class of compounds, observed as intermediates in various reactions. However, in the last decades, a class of carbenes, namely *N*-Heterocyclic Carbenes (NHCs) that show high stability at room temperature and under air conditions have been developed.

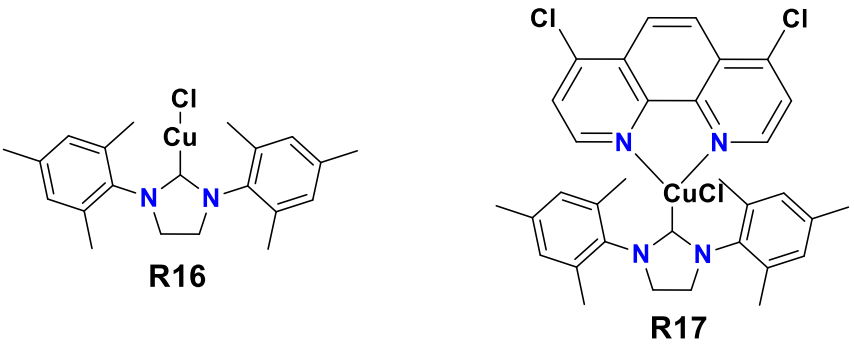

Figure 3.3 Copper(I) heterocyclic carbenes used for CuAAC reactions

Compared to the classic copper (I) catalysts for CuAAC reactions, Cu(I)-NHC catalysts are very stable, inert conditions for the reactions performed under their catalysis or for storage not being necessary. They are also very efficient when deployed in CuAAC reactions. The results provided by **R16** are less enthusiastic, but transformed *in situ*[44] or pre-reaction[45] in **R17** type complexes with pyridine type ligands they yield very good results.

3.2 Results and discussion

Given the versatility of the rotaxanes to act as molecular machines triggered by a variety of stimuli, as well as the increasing number of their potential applications we have decided to develop rotaxanes by following a new synthetic approach, namely metal active clipping with active metal coordination site located on the axle (**Figure 3.4**).

Our method combines previously described clipping and the metal active template methods. As shown in the introduction section metal active template method uses a metal ion-macrocycle complex which catalyzes the formation of the axle and implicitly of the [2]rotaxane (**Figure 3.4, right**). It is also most often coupled with a CuAAC click reaction, which proceeds with very good yields of 60-90% and has been also successfully used for the synthesis of chiral [2]rotaxanes obtain from chiral starting materials.[46]

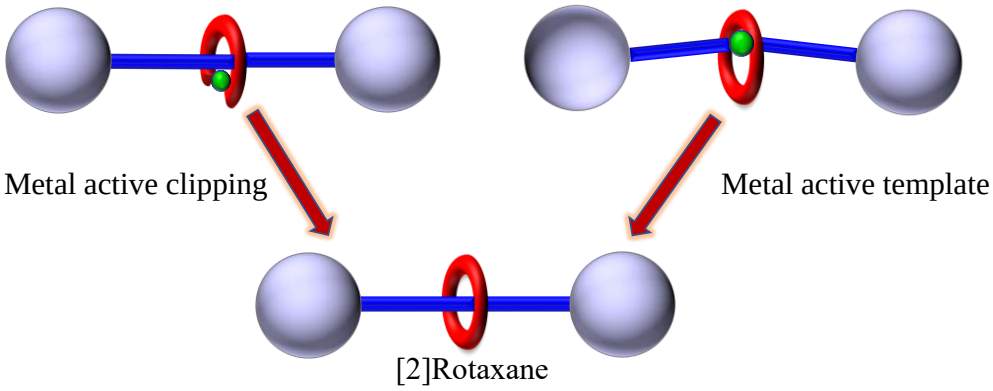

Figure 3.4 Metal active clipping (used in this work) and metal active template methods

In order to achieve the target [2]rotaxane by our method, the metal ion is connected to the dumbbell-shaped molecule through a coordination bond. The metal-ion catalyzes the macrocyclization reaction around the axle.

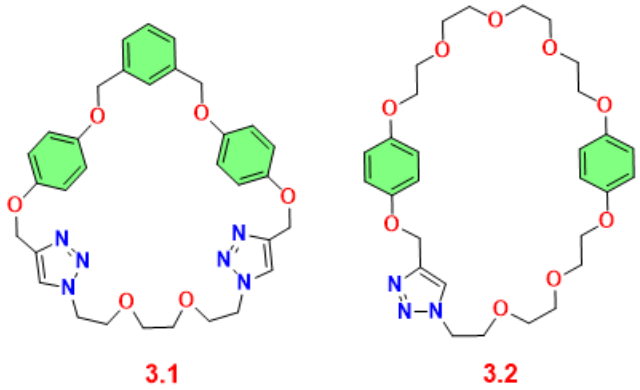

Figure 3.5 The macrocyclic components of the [2]rotaxanes

The design of axle for [2]rotaxanes (**Figure 3.10**) includes tetraarylmethane based stoppers, a pyridine station for metal coordination, as well as two triazole moieties which can be transformed after *N*-alkylation into triazolium stations. Having in mind the efficiency of the CuAAC click reaction, we have decided to apply it not only for the clipping reaction, but also for the formation of the dumbbell-shaped molecule.

Due to the poor results obtained during the synthesis of the first rotaxane **3.3**, which might be attributed to the possible coordination of the triazole moieties to the copper (I),[47] we have inserted a phenyl spacer between the pyridine and the triazole in order to decrease the likelihood of such event.

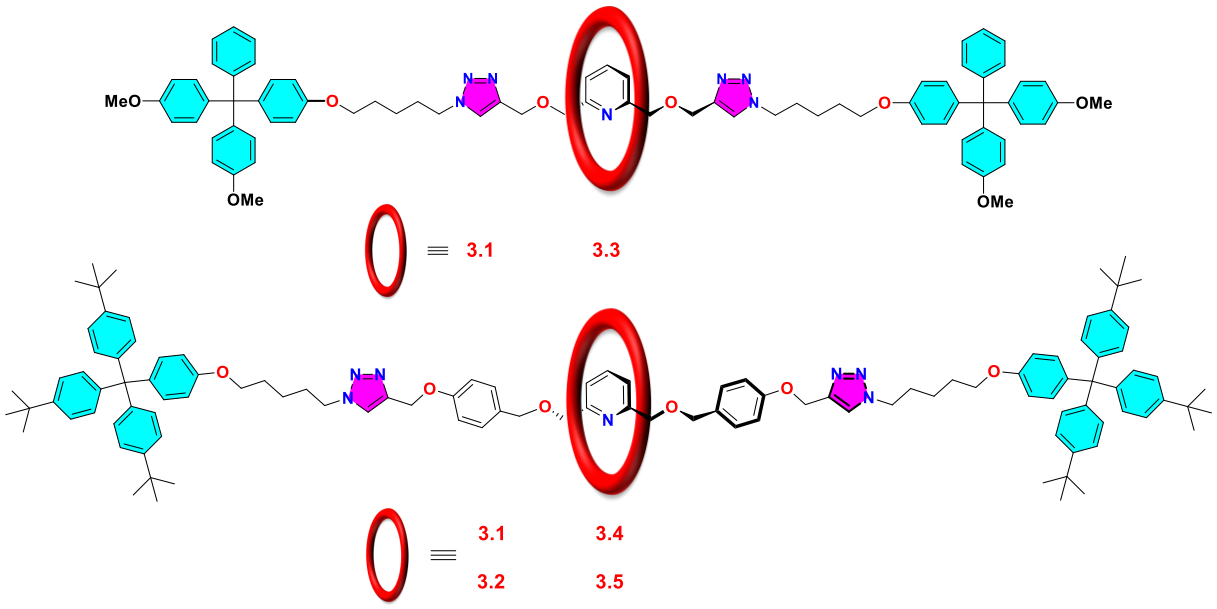

Figure 3.6 The structure of the target [2]rotaxanes

3.2.1 The synthesis of [2]rotaxane precursors

3.2.1.1 The synthesis of the stoppers

For the synthesis of the stoppers we have used two tetraarylmethane bulky fragments, the first one is based on 4,4'-dimethoxytrityl moiety which is usually used as a protecting group for alcohols[48] and was readily available in our laboratory. The second stopper based on tris(4-tert-butylphenyl)methane is widely used in the synthesis of MIMs because of its symmetry which results in simpler NMR spectra. The actual synthesis of the stopper involved the formation of the tetraarylmethane fragment (compounds **3.8** in **Scheme 3.1**), followed by the attachment of a pentyl linker and its functionalization with azide group (**Scheme 3.1**).

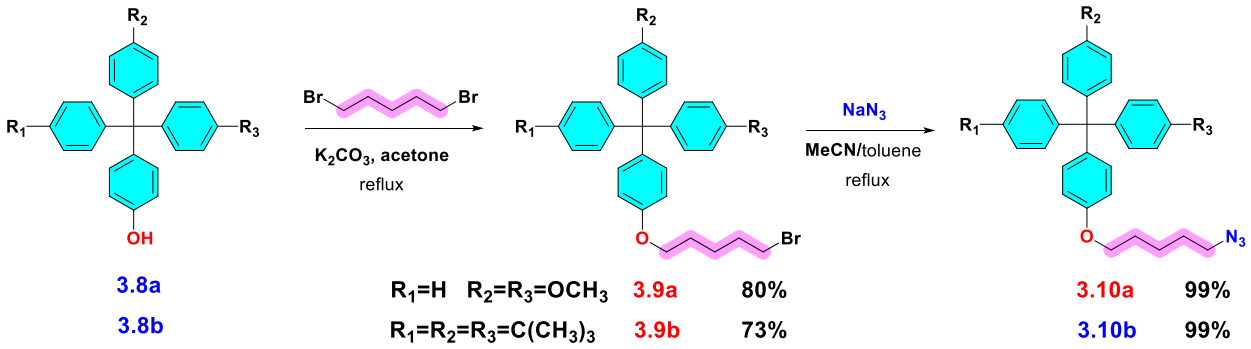

Scheme 3.1 The transformation of the tritylphenols into azides

3.2.1.2 The synthesis of the pyridine station

The synthesis of dialkyne **3.11** was again straightforward, a phase-transfer, tetra-n-butylammonium bromide (TBAB) catalyzed SN_2 reaction. In the case of compound **3.11a**, the intramolecular hydrogen bond between the hydroxyl and the pyridine nitrogen in the diol limits the yield of the reaction. A better alternative could be used (e.g. formation of the alkoxide in presence of NaH) for large scale amounts, but the quantity obtained was sufficient for our purpose.

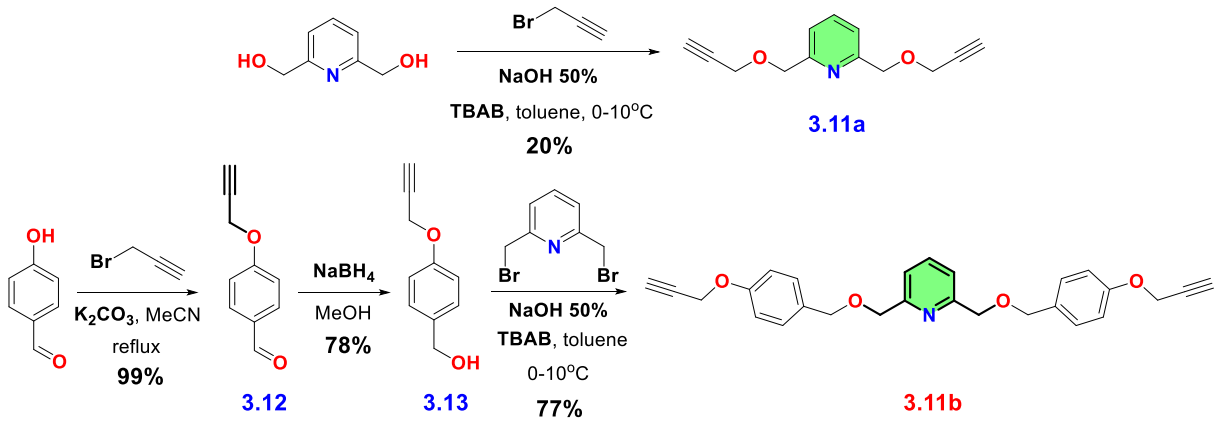

Scheme 3.2 Synthesis of the pyridine containing dialkynes

3.2.1.3 The synthesis of the dumbbell-shaped molecules

With both the dialkynes and the diazides in hand we have performed the CuAAC click reaction to form the dumbbell-shaped molecules **3.14** (**Schemes 3.3** and **3.4**). Both reactions are catalyzed by Cu(I), but in the first case the catalyst was obtained *in situ* by the reduction of Cu(II) with sodium ascorbate used in excess (10 eq.). In order to have an efficient reaction, tris((1-benzyl-4-triazolyl)methyl)amine (TBTA) is added to stabilize and enhance the catalytic activity of Cu(I).

For synthesis of **3.14b**, we have decided to use a CuNHC catalyst, namely **3.15(phen)**, which was provided by Dr. Arnaud Gautier from Université Clermont Auvergne. This catalyst is stable, under air atmosphere, both in solid state as well as in solution and efficiently catalyzed our reaction yielding 95% of the target compound **3.14b**. The impressive catalytic activity of this type of CuNHC and the displayed stability are the main reasons behind our decision to apply it to the formation of rotaxanes by metal active clipping reactions.

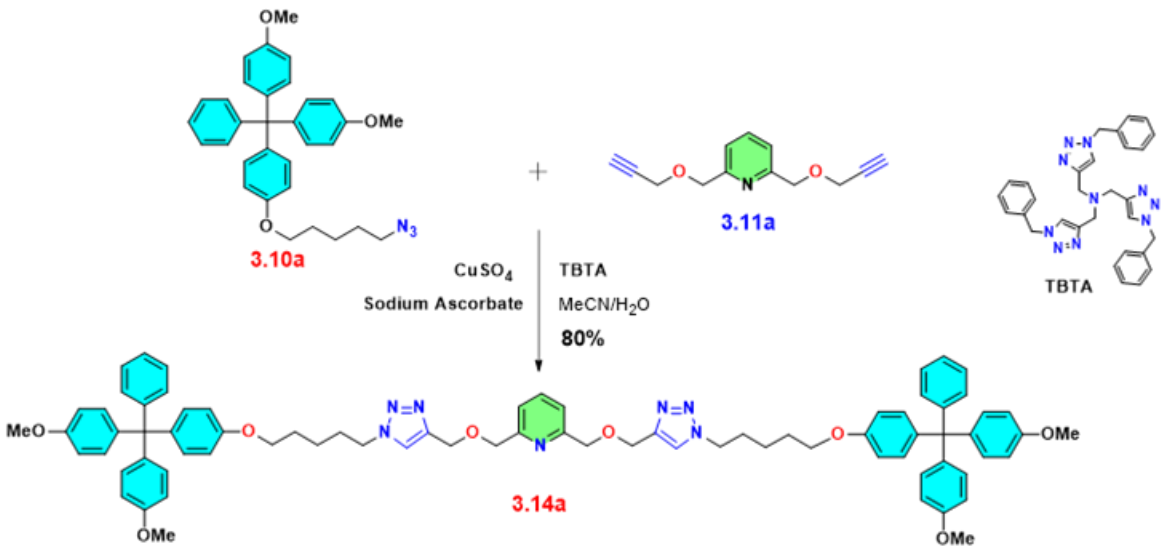

Scheme 3.3 The synthesis of our first dumbell-shaped molecule **3.14a**

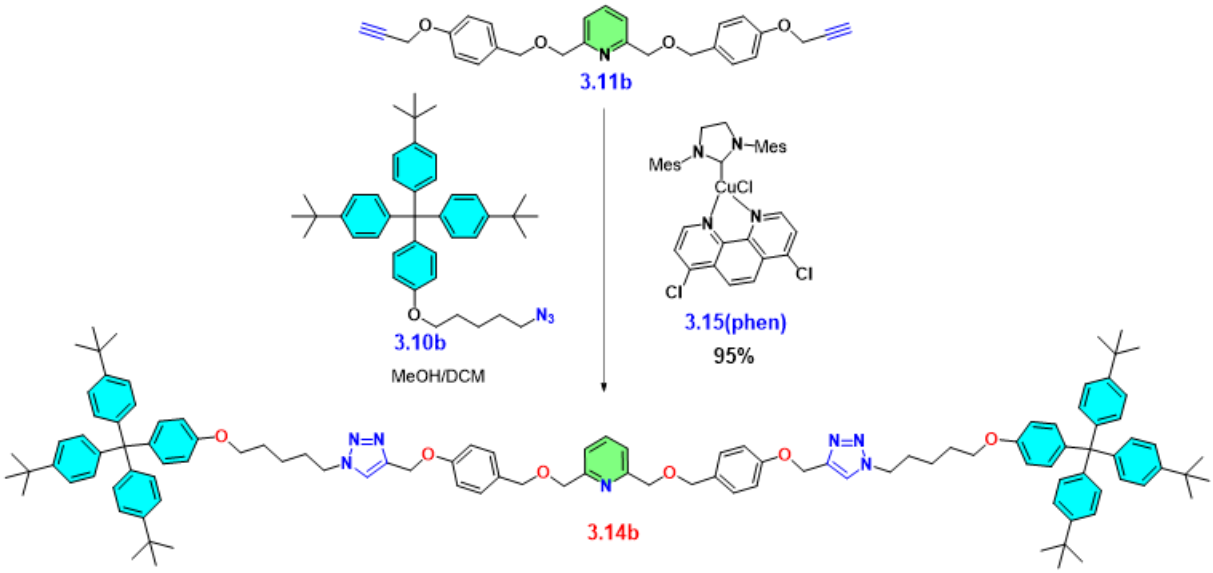

Scheme 3.4 The synthesis of the second dumbell-shaped molecule **3.14b**

3.2.1.4 The synthesis of macrocycle precursors and of the macrocycles

The structures of the target macrocycles **3.1** and **3.2** share two important functional groups, which leads to similarities in the synthesis of the precursors and macrocycles themselves, namely the triazole and the ethyleneglycole moieties. While compound **3.1** is symmetric and is more easily accessible (**Scheme 3.5**) in only 5 steps, compound **3.2** is unsymmetric and its synthetic strategy is more complicated involving 9 steps.[49] In both cases the last reaction is a

CuAAC macrocyclization *click* reaction catalyzed by **3.15(phen)**, which requires high dilution in order to obtain a satisfying yield.

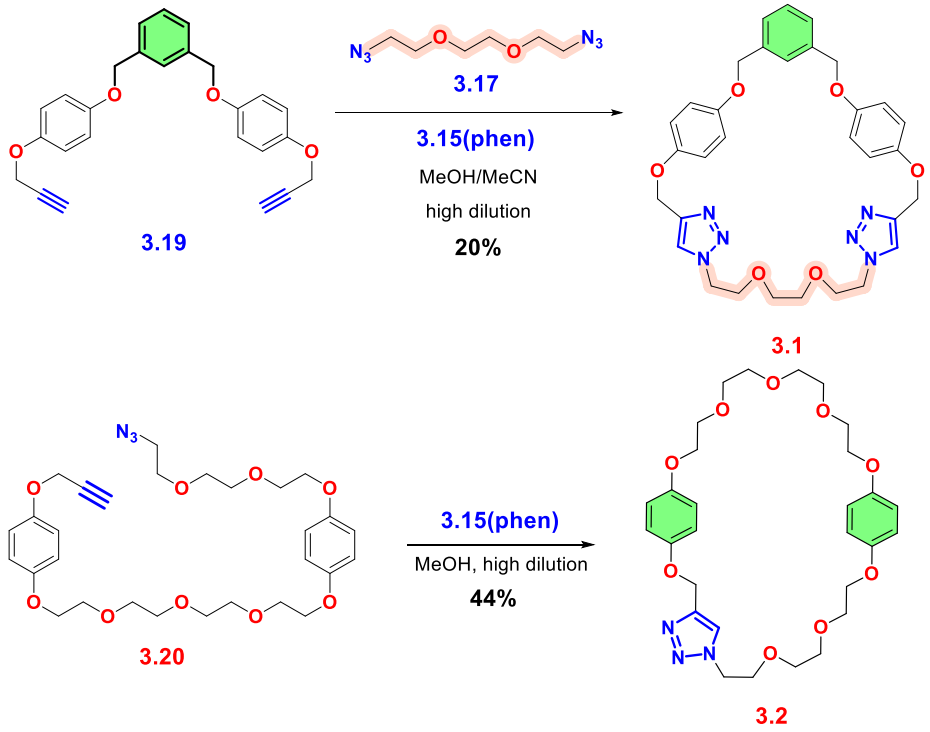

Scheme 3.5 The synthesis of the macrocycles **3.1** and **3.2**

3.2.2 The synthesis of the rotaxanes 3.3 and 3.4 in a "two components" click reaction

The clipping reactions were performed first from stock solutions of **3.14a**, **3.19**, **3.17** and of $Cu(CH_3CN)_4PF_6$ in MeCN, and of **3.15** in MeOH (**Scheme 3.6**).

The presence of the rotaxane in the reaction mixture was confirmed by HRMS. The MS spectrum of method **A** displayed a more intense ionization peak corresponding to the rotaxane **3.3**. This information corroborated with the inert conditions required by the commercial catalyst, turned our focus toward the NHC based catalyst, which could be left for days to react under normal conditions.

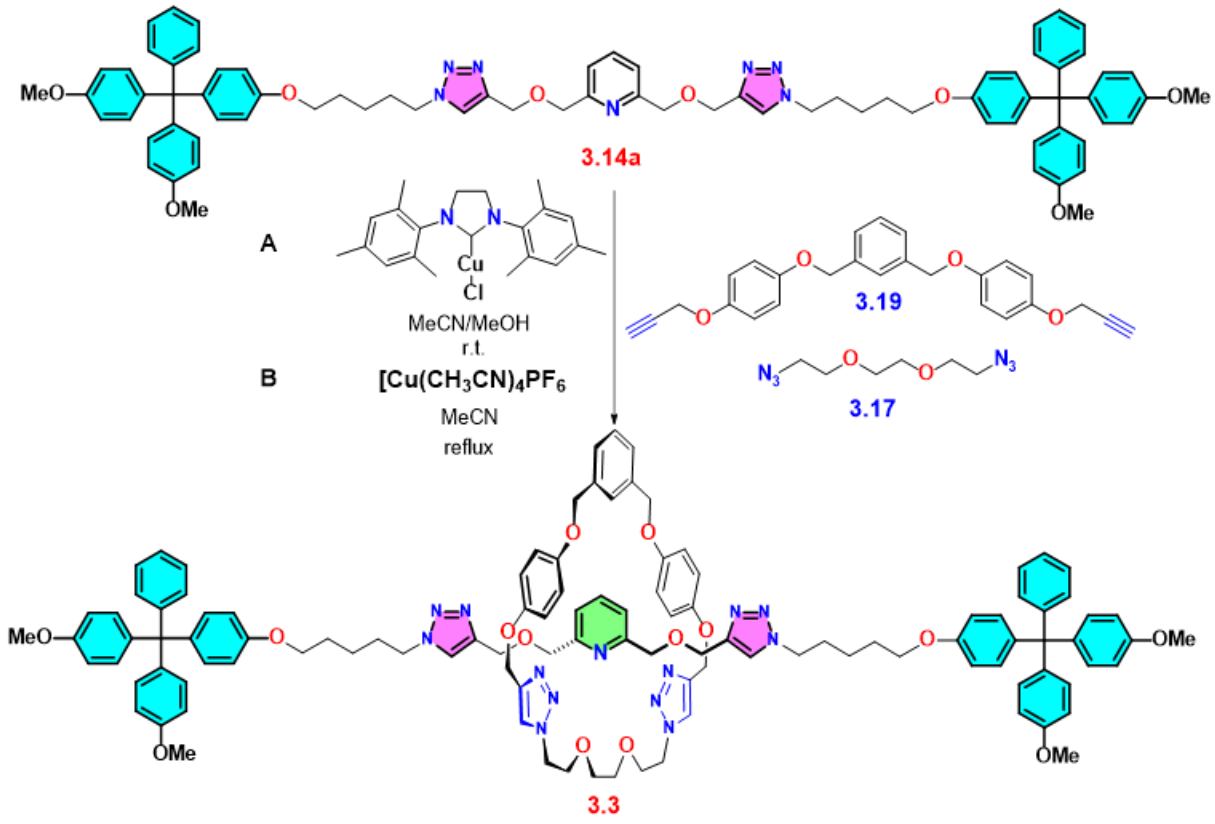

Scheme 3.6 The synthesis of rotaxane **3.3** with CuCl(SIMes) (method A) or $Cu(CH3CN)_4PF_6$ (method B)

Because of that, our next natural step was to apply the macrocyclization reaction to axle **3.14b** with rotaxane **3.4** as our target, counting on the phenyl spacer to improve the [2]rotaxane formation.

Despite our efforts, rotaxane **3.4** proved as elusive as its predecessor. The spacer did not seem to have an enough effect on the activity of the catalyst for the formation of the rotaxane.

3.2.3 The synthesis and characterization of rotaxane 3.5

In order to have a chance at isolating the [2]rotaxane from our clipping reaction, we have used an intramolecular macrocyclization reaction, which was performed from compound **3.20** (**Scheme 3.7**). This allowed the isolation of rotaxane in 3% yield.

The superposition of the ^{1}HNMR spectra of the components and the rotaxane shows a small shielding of all the axle protons. The macrocycle's signals are more shifted, with the triazole proton presenting an upfield shift from δ= 7.95 ppm to δ= 7.65 ppm and the hydroquinone protons an upfield shift from δ= 6.77/6.67 ppm to δ= 6.60/6.58 ppm (**Figure 3.7**).

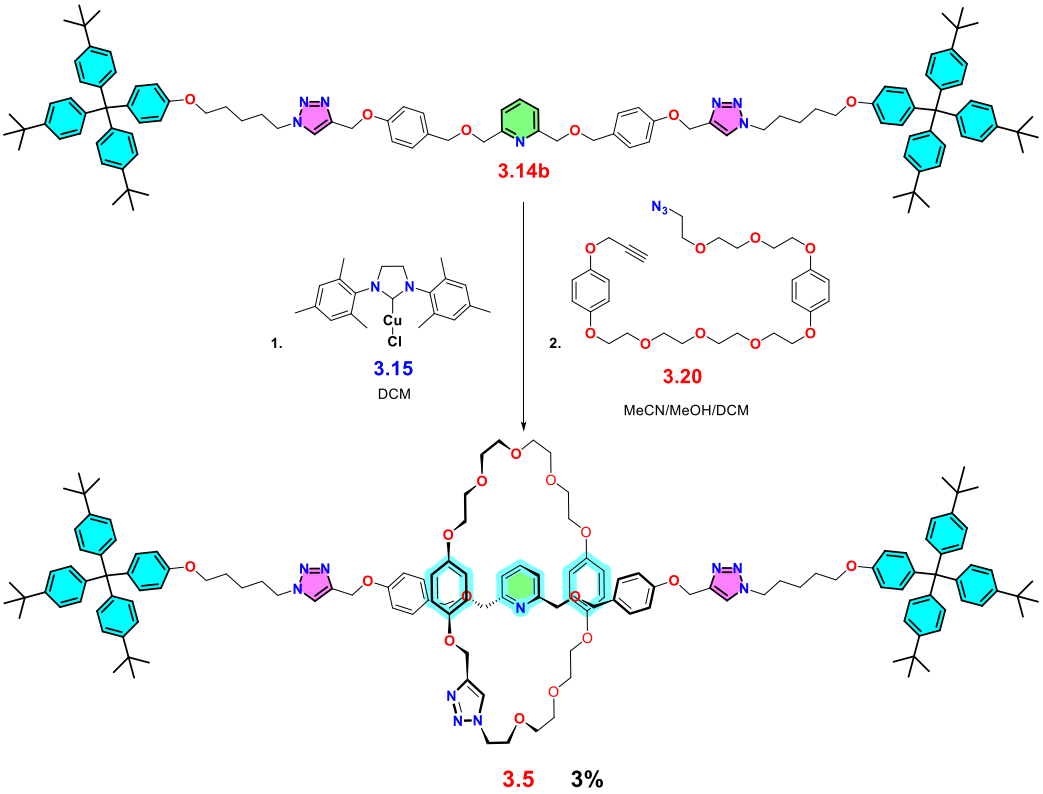

Scheme 3.7 The synthesis of rotaxane **3.5** with CuCl(SIMes)

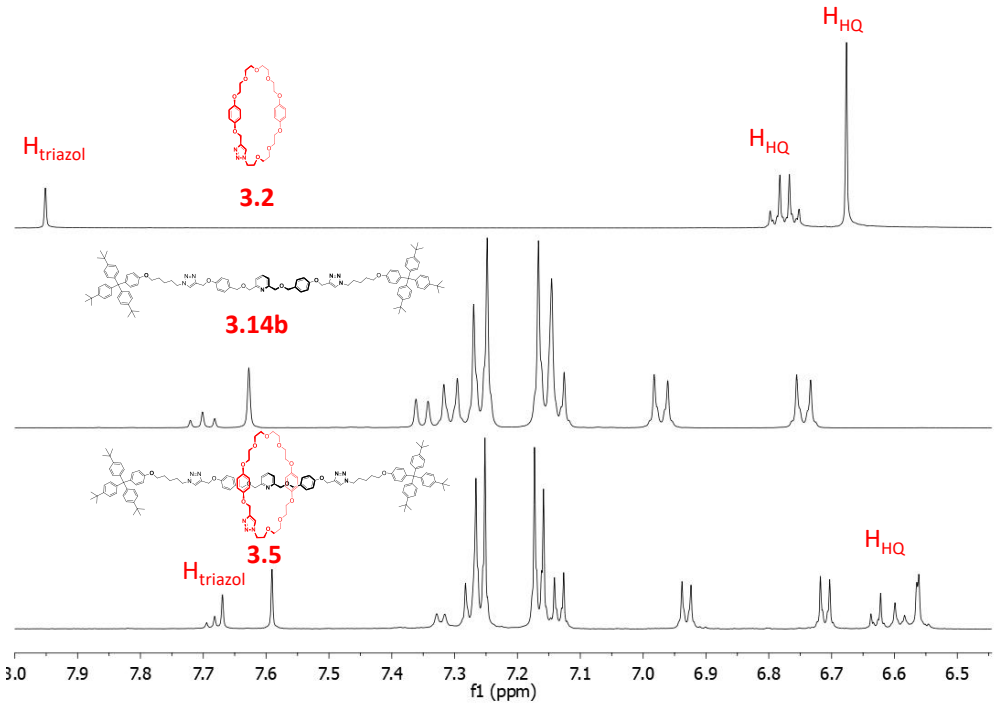

Figure 3.7 Comparative 1HNMR spectra of the aromatic region of rotaxane **3.5** with the macrocycle and with the axle (CD_2Cl_2, 400MHz)

3.3 Conclusions

In conclusion, we have produced three novel mechanically interlocked molecules, [2]rotaxanes, by following a new imaginative method, metal active clipping reaction. As proof of concept, this method didn not give the best results, and further improvements could be thought and applied. The first two [2]rotaxanes **3.3** and **3.4**, with different axles, couldn't be isolated, but their formation was confirmed by HRMS spectra. This unsuccess could be attributed to the design of the macrocycle **3.1**, formed by a [1+1] macrocyclization. Rotaxane **3.5** was isolated after the design of the macrocycle was changed. The final step of the method was an intramolecular macrocyclization, from precursor **3.20**. The structure of the compound was validated by TLC, HRMS and NMR measurements.

Our research proved the efficiency of CuAAC click reactions catalyzed by copper(I) *N*-heterocyclic carbenes in the synthesis of [2]rotaxanes. This combined with the fast and simple assembly of [CuCl(SIMes)] could lead to development of a CuNHC click chemistry in MIMs domain.

General conclusions

The attempted synthesis of a new rigidified terthiophene based NFA led us to the unexpected formation of a naphto[2,3-thiophene] derivative **1.2b**, which was confirmed by NMR, HRMS and X-ray diffraction on single crystal. We have also synthesized and characterized a new series of terthiophene diesters and hexathiophene tetraesters. Initially the compounds were designed with methyl ester, but the low solubility of compound **1.3a** lead to the hexyl target compounds **1.3b-d**. The poor efficiencies of **1.3b** and **1.3c** OSCs, and the better efficiency 1.72% PCE of **1.3d** OSC lead to the design of **1.4a** and **1.4b**. The lengthening of the thiophene chain didn't bring any new improvement.

Contributions to the synthesis and characterization of some D-A triarylamine donors, which were used as single materials for OSCs, were also presented. While a clear understanding of the functioning of this type of material is still to be formulated, we believe that our results are an important stepping stone towards explaining the mechanism behind this type of SMOSCs.

The absorption and emission behavior of a series of 1,3,4-oxadiazole containing compounds, that were synthesized during the master studies, was analyzed. This indicated the

influence of the solvent as well as of hydrogen bonding on the emission properties through ESIPT (for compounds **2.2a** and **2.2b**) and ESPT processes both in solution and in solid state. Moreover, the investigated compounds were successfully used in co-crystallization experiments with pyridine derivatives.

The same analysis was performed for another series of bis-oxadiazoles, that were synthesized by Drd. Codruța Bădescu during her master. Their spectra display emission maxima in the green region for the unprotected compounds and in the blue region for the protected compound. The optical parameters are visibly different from those showed by compounds **2.1** and **2.2**, with Stokes shifts higher than 15000 cm^{-1} and very high quantum yields. The structural particularities of the newly synthesized compounds do not allow intramolecular fluorescence quenching and the quantum yields are almost half of the value of the fluorescein standard for the green-emissive compounds (**2.3**) and almost equal to the value of the quinine, for the blue-emissive, benzyl-protected compounds (**2.4**). In solid state, compound **2.3a** is very luminescent compared to compound **2.3b**, proving the importance of tertbutyl instead of methyl as a substituent.

We have obtained three novel mechanically interlocked molecules, [2]rotaxanes, by following a new imaginative method, metal active clipping reaction. The first two [2]rotaxanes **3.3** and **3.4**, with different axles, couldn't be isolated, but their formation was confirmed by HRMS spectra. The modification of the macrocycle, formed by an intramolecular reaction, allowed the isolation of rotaxane **3.5**. This was confirmed by NMR and HRMS measurements. This research offers a new way of applying CuAAC click reactions in the synthesis of [2]rotaxanes.

Bibliography

1 K. E. Dalle, J. Warnan, J. J. Leung, B. Reuillard, I. S. Karmel and E. Reisner, *Chem. Rev.*, 2019, **119**, 2752–2875.

2 G. Zhang, J. Zhao, P. C. Y. Chow, K. Jiang, J. J. Zhang, Z. Zhu, J. J. Zhang, F. Huang and H. Yan, *Chem. Rev.*, 2018, **118**, 3447–3507.

3 A. Wadsworth, M. Moser, A. Marks, M. S. Little, N. Gasparini, C. J. Brabec, D. Baran and I. McCulloch, *Chem. Soc. Rev.*, 2019, **48**, 1596–1625.

4 C. C. Anghel, I. Stroia, A. Pop, A. Bende, I. Grosu, N. D. Hădade and J. Roncali, *RSC Adv.*, 2021, **11**, 9894–9900.

5 A. Leliège, C. H. Le Régent, M. Allain, P. Blanchard and J. Roncali, *Chem. Commun.*, 2012, **48**, 8907–8909.

6 N. Terenti, G.-I. Giurgi, A. P. Crişan, C. Anghel, A. Bogdan, A. Pop, I. Stroia, A. Terec, L. Szolga, I. Grosu and J. Roncali, *J. Mater. Chem. C*, 2022, **10**, 5716–5726.

7 C. Anghel, M. Matache, C. C. Paraschivescu, A. M. Madalan and M. Andruh, *Inorg. Chem. Commun.*, 2017, **76**, 22–25.

8 A. Yoshimura and V. V. Zhdankin, *Chem. Rev.*, 2016, **116**, 3328–3435.

9 C. C. Paraschivescu, M. Matache, C. Dobrotaì, A. Nicolescu, C. Maxim, C. Deleanu, I. C. Faìrcaìsìanu and N. D. Haìdade, *J. Org. Chem.*, 2013, **78**, 2670–2679.

10 W. Yu, G. Huang, Y. Zhang, H. Liu, L. Dong, X. Yu, Y. Li and J. Chang, *J. Org. Chem.*, 2013, **78**, 10337–10343.

11 C. C. Anghel, C. Bădescu, A. G. Mirea, N. D. Hădade, A. M. Mădălan, M. Matache and C. C. Popescu, *Dye. Pigm.*, 2022, **197**, 109927.

12 C. C. Paraschivescu, N. D. Hədade, A. G. Coman, A. Gautier, F. Cisnetti and M. Matache, *Tetrahedron Lett.*, 2015, **56**, 3961–3964.

13 A. D. Beldovskaya, G. A. Dushenko, N. I. Vikrishchuk, L. D. Popov, Y. V. Revinskii, I. E. Mikhailov and V. I. Minkin, *Russ. J. Org. Chem.*, 2013, **49**, 1861–1863.

14 S. Ma, S. Du, G. Pan, S. Dai, B. Xu and W. Tian, *Aggregate*, 2021, **2**, e96.

15 Y. Wang, W. Zhu, H. Dong, X. Zhang, R. Li and W. Hu, *Top. Curr. Chem.*, 2016, **374**, 1–34.

16 M. Răducă and A. M. Mădălan, *Crystals*, 2021, **11**, 1217.

17 A. G. Coman, A. Paun, C. C. Popescu, N. D. Hădade, C. C. Anghel, A. M. A. M. Mădălan, P. Ioniţă and M. Matache, *New J. Chem.*, 2018, **42**, 14111–14119.

18 A. O. Doroshenko, E. A. Posokhov, A. A. Verezubova and L. M. Ptyagina, *J. Phys. Org. Chem.*, 2000, **13**, 253–265.

19 J. Seo, S. Kim, Y. S. Lee, O. H. Kwon, K. H. Park, S. Y. Choi, Y. K. Chung, D. J. Jang and S. Y. Park, *J. Photochem. Photobiol. A Chem.*, 2007, **191**, 51–58.

20 L. Chen, P. Y. Fu, H. P. Wang and M. Pan, *Adv. Opt. Mater.*, 2021, **9**, 2001952.

21 M. Xue, Y. Yang, X. Chi, X. Yan and F. Huang, *Chem. Rev.*, 2015, **115**, 7398–7501.

22 F. Coutrot, *ChemistryOpen*, 2015, **4**, 556–576.

23 A. Diac, M. Matache, I. Grosu and N. D. Hădade, *Adv. Synth. Catal.*, 2018, **360**, 817–845.

24 É. M. Foyle and N. G. White, *Chem. – Asian J.*, 2021, **16**, 575–587.

25 N. H. Evans, *Eur. J. Org. Chem.*, 2019, **2019**, 3320–3343.

26 X. Han, G. Liu, S. H. Liu and J. Yin, *Org. Biomol. Chem.*, 2016, **14**, 10331–10351.

27 A. Inthasot, S. Te Tung and S. H. Chiu, *Acc. Chem. Res.*, 2018, **51**, 1324–1337.

28 J. E. Beves, B. A. Blight, C. J. Campbell, D. A. Leigh and R. T. McBurney, *Angew. Chem. Int. Ed.*, 2011, **50**, 9260–9327.

29 I. Yoon, M. Narita, T. Shimizu and M. Asakawa, *J. Am. Chem. Soc.*, 2004, **126**, 16740–16741.

30 S. Y. Hsueh, J. L. Ko, C. C. Lai, Y. H. Liu, S. M. Peng and S. H. Chiu, *Angew. Chem. Int. Ed.*, 2011, **50**, 6643–6646.

31 C. W. Chiu, C. C. Lai and S. H. Chiu, *J. Am. Chem. Soc.*, 2007, **129**, 3500–3501.

32 B. Taghavi Shahraki, S. Maghsoudi, Y. Fatahi, N. Rabiee, S. Bahadorikhalili, R. Dinarvand, M. Bagherzadeh and F. Verpoort, *Coord. Chem. Rev.*, 2020, **423**, 213484.

33 S. D. P. Fielden, D. A. Leigh, C. T. McTernan, B. Pérez-Saavedra and I. J. Vitorica-Yrezabal, *J. Am. Chem. Soc.*, 2018, **140**, 6049–6052.

34 G. De Bo, G. Dolphijn, C. T. McTernan and D. A. Leigh, *J. Am. Chem. Soc.*, 2017, **139**, 8455–8457.

35 J. F. Stoddart, *Angew. Chem. Int. Ed.*, 2017, **56**, 11094–11125.

36 S. Erbas-Cakmak, D. A. Leigh, C. T. McTernan and A. L. Nussbaumer, *Chem. Rev.*, 2015, **115**, 10081–10206.

37 H. Y. Zhou, Y. Han and C. F. Chen, *Mater. Chem. Front.*, 2019, **4**, 12–28.

38 M. Baroncini, M. Canton, L. Casimiro, S. Corra, J. Groppi, M. La Rosa, S. Silvi and A. Credi, *Eur. J. Inorg. Chem.*, 2018, **2018**, 4589–4603.

39 B. Yao, H. Sun, L. Yang, S. Wang and X. Liu, *Front. Chem.*, 2022, **9**, 1236.

40 S. Yu, N. D. McClenaghan and J. L. Pozzo, *Photochem. Photobiol. Sci.*, 2019, **18**, 2102–2111.

41 M. Baroncini, S. Silvi and A. Credi, *Chem. Rev.*, 2020, **120**, 200–268.

42 H. V. Schröder and C. A. Schalley, *Chem. Sci.*, 2019, **10**, 9626–9639.

43 K. M. Bąk, K. Porfyrakis, J. J. Davis and P. D. Beer, *Mater. Chem. Front.*, 2020, **4**, 1052–1073.

44 M. L. Teyssot, A. Chevry, M. Traïkia, M. El-Ghozzi, D. Avignant and A. Gautier, *Chem. – Eur. J.*, 2009, **15**, 6322–6326.

45 M. L. Teyssot, L. Nauton, J. L. Canet, F. Cisnetti, A. Chevry and A. Gautier, *Eur. J. Org. Chem.*, 2010, **2010**, 3507–03515.

46 M. A. Jinks, A. de Juan, M. Denis, C. J. Fletcher, M. Galli, E. M. G. Jamieson, F. Modicom, Z. Zhang and S. M. Goldup, *Angew. Chem. Int. Ed.*, 2018, **57**, 14806–14810.

47 A. Noor, J. E. M. Lewis, S. A. Cameron, S. C. Moratti and J. D. Crowley, *Supramol. Chem.*, 2012, **24**, 492–498.

48 S. Shahsavari, J. Chen, T. Wigstrom, J. Gooding, A. Gauronskas and S. Fang, *Tetrahedron Lett.*, 2016, **57**, 3877–3880.

49 T. A. Cucuiet, C. C. Anghel, E. Bogdan, A. Crişan, M. Matache, L. Pop, A. Terec and N. D. Hădade, *Rev. Roum. Chim.*, 2020, **65**, 567–572.

List of publications

1. *Click synthesis and complexation properties of a new unsymmetrical macrocycle bearing 1,4-dioxabenzene and triazole units*

Teodor A. Cucuiet, **Cătălin C. Anghel**, Elena Bogdan, Andreea Crișan, Mihaela Matache, Lidia Pop, Anamaria Terec, Niculina D. Hădade

Revue Roumaine de Chimie, 2020, 65(6), 567-572.

2. *An attempt to synthesize a terthienyl-based analog of indacenedithiophene (IDT): unexpected synthesis of a naphtho[2,3-b]thiophene derivative*

Cătălin C Anghel, Ioan Stroia, Alexandra Pop, Attila Bende, Ion Grosu, Niculina D. Hădade, Jean Roncali

RSC Advances, 2021, 11, 9894-9900.

3. *Two are better than one - Synthesis of novel blue and green emissive hydroxy-oxadiazoles*

Cătălin C. Anghel, Codruța Bădescu, Anca G. Mirea, Niculina D. Hădade, Augustin M. Mădălan, Mihaela Matache, Codruța C. Popescu

Dyes and Pigments, 2022, 197, 109927.

4. *Structure-properties of small donor-acceptor molecules for homojunction single-material organic solar cells*

Natalia Terenti, Gavril-Ionel Giurgi, Andreea Petronela Crișan, **Cătălin C. Anghel**, Alexandra Bogdan, Alexandra Pop, Ioan Stroia, Anamaria Terec, Lorant Szolga, Ion Grosu, Jean Roncali

Journal of Materials Chemistry C, 2022, 10, 5716-5726.

5. *Shifting emission of oxadiazoles via inter- or intramolecular hydrogen bonding*

Cătălin C. Anghel, Anca G. Mirea, Codruța C. Popescu, Augustin Mădălan, Anamaria Hanganu, Attila Bende, Niculina D. Hădade, Mihaela Matache, Marius Andruh

Submitted.